Volume 5
Number 2
February 2026
Pages 109–262

Sensors & Diagnostics

rsc.li/sensors

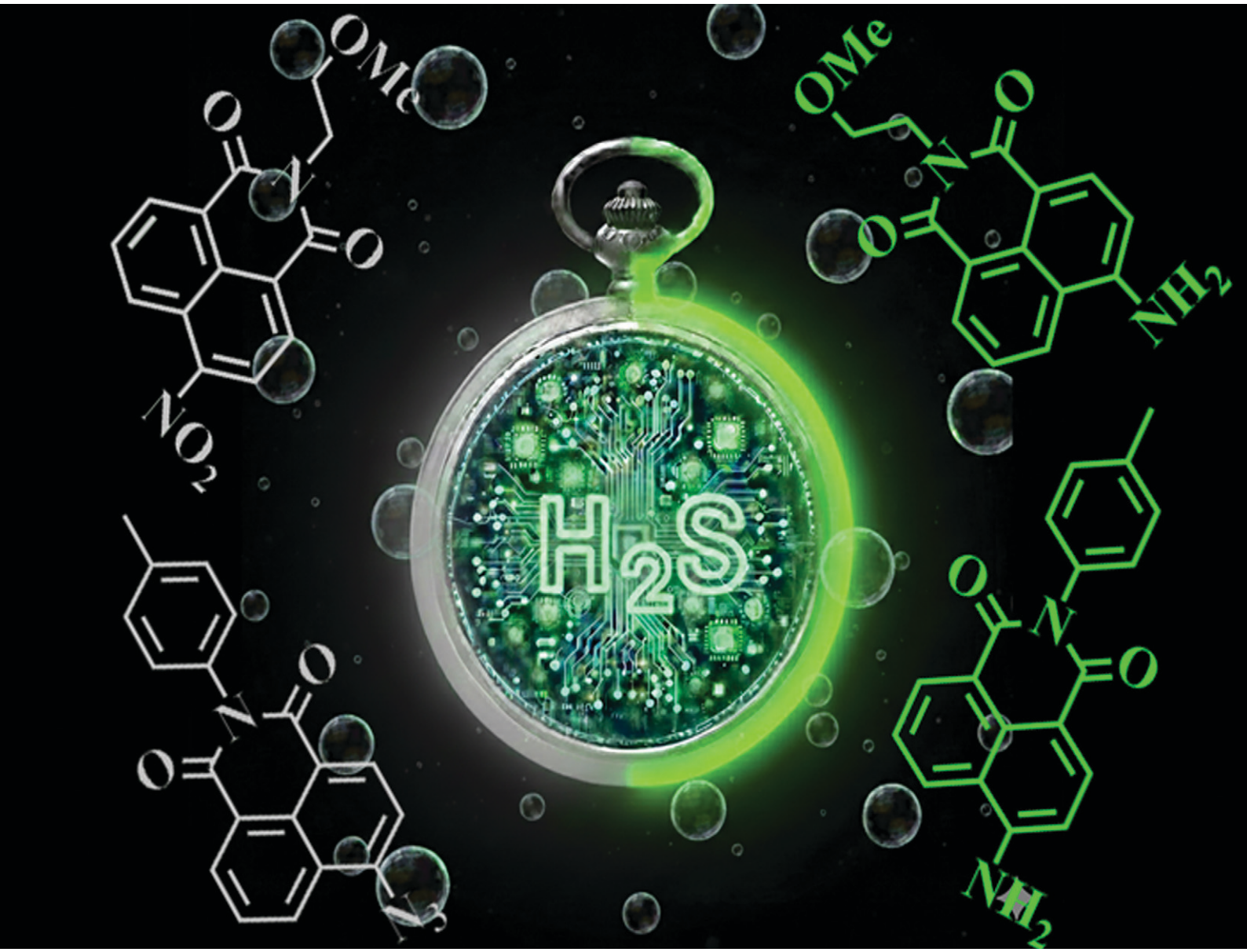

ISSN 2635-0998

ROYAL SOCIETY OF CHEMISTRY

TUTORIAL REVIEW

Sankarasekaran Shanmugaraju *et al.*

1,8-Naphthalimide-derived reactivity-based fluorescent probes for detection and imaging of H_2S

Sensors & Diagnostics

TUTORIAL REVIEW

View Article Online
View Journal | View Issue

Cite this: *Sens. Diagn.*, 2026, **5**, 184

1,8-Naphthalimide-derived reactivity-based fluorescent probes for detection and imaging of H_2S

Mannanthara Kunhumon Noushija, Alenthwar Vamshi Krishna and Sankarasekaran Shanmugaraju *

Hydrogen sulfide (H_2S) is both an important biological signaling molecule and a toxic environmental pollutant, making its precise detection essential for biomedical research and environmental monitoring. Among the various sensing platforms available, amino-1,8-naphthalimide (**Nap**)-based fluorescent probes have become powerful tools for real-time H_2S detection due to their high sensitivity, excellent selectivity, biocompatibility, and quick response. **Nap** fluorophores offer several inherent advantages—including strong and tunable emission, prominent intramolecular charge-transfer (ICT) characteristics, large Stokes shifts, and easy structural modification—making them especially attractive as scaffolds for developing activity-based probes. This review highlights recent developments in **Nap**-derived fluorescent sensors for H_2S detection, categorizing the probes based on their reactive sites and sensing mechanisms, such as thiolysis, reduction, and nucleophilic substitution. For each category, we explore structure–function relationships, photophysical properties, sensing performance, and practical applications in biological and environmental settings. Finally, we address current challenges and future directions in designing next-generation **Nap**-based probes with enhanced ratiometric responses, targeted subcellular localization, two-photon excitation capabilities, and improved suitability for *in vivo* imaging. Overall, this review offers a comprehensive perspective to guide the rational development of innovative fluorescent tools for accurate and efficient H_2S detection.

Received 6th November 2025,
Accepted 16th January 2026

DOI: 10.1039/d5sd00201j

rsc.li/sensors

1. Introduction

Gasotransmitters are a distinct class of endogenously produced gaseous molecules that play pivotal roles in diverse physiological functions.[1] The classical gasotransmitter family comprises carbon monoxide (CO), nitric oxide (NO), and hydrogen sulfide (H_2S).[2] Among them, H_2S has attracted particular attention and has historically been recognized for its characteristic odour of rotten eggs and cytotoxic effects. H_2S is now appreciated as a biologically relevant signalling molecule with implications in both health and disease.[3–6]

Department of Chemistry, Indian Institute of Technology Palakkad, Palakkad-678623, Kerala, India. E-mail: shanmugam@iitpkd.ac.in

Mannanthara Kunhumon Noushija

Ms. Mannanthara Kunhumon Noushija obtained her B.Sc. in Chemistry from Government Victoria College, Palakkad (2018), and subsequently completed her M. Sc. in Chemistry at the University of Calicut, Thenhippalam (2020). She is currently pursuing her Ph.D. in the Department of Chemistry at the Indian Institute of Technology Palakkad, where her research centers on the development of small-molecule fluorescent chemosensors for biologically relevant analytes.

Alenthwar Vamshi Krishna

Mr. Alenthwar Vamshi Krishna received his BS-MS dual degree in Chemistry in 2019 from the Indian Institute of Science Education and Research (IISER) Pune. He is currently pursuing his Ph.D. in the Department of Chemistry at the Indian Institute of Technology Palakkad. His research focuses on the design and development of organic cathode materials for advanced energy storage applications.

Notably, unlike CO and NO, H_2S exhibits high water solubility, which confers unique biological properties.[7] In mammalian systems, endogenous H_2S is primarily synthesized through the enzymatic activities of cystathionine β-synthase (CBS), cystathionine γ-lyase (CSE), and 3-mercaptopyruvate sulfurtransferase (3MST).[8–11] The abundance of H_2S in biological systems varies depending on the enzymatic pathway involved, the organism, the tissue type, and the prevailing physiological state.[12] Additionally, bacterial metabolism contributes to H_2S production inside the body, while in the environment, H_2S is generated as a by-product of several industrial activities, particularly within petroleum-related sectors.[13]

Subsequent research has demonstrated that H_2S exerts multiple physiological effects, including regulation of vascular tone, anti-inflammatory activity, neuroprotection, antioxidant defense, and modulation of mitochondrial bioenergetics.[2–6,14] These physiological functions highlight the critical role of H_2S in maintaining homeostasis and protecting against disorders such as hypertension, neurodegeneration, and cardiovascular disease.[11,15–18] In contrast, abnormal H_2S levels have been associated with central nervous system diseases, including Down's syndrome, Alzheimer's disease, and Parkinson's disease.[19–22] Taken together, current evidence positions H_2S as a critical endogenous gasotransmitter with broad physiological relevance and potential therapeutic significance. Therefore, accurate and timely monitoring of H_2S levels under both physiological and pathological conditions as well as within biological systems is critically important.

The detection of H_2S has traditionally relied on a range of analytical platforms, including chromatographic techniques such as high-performance liquid chromatography (HPLC) and gas chromatography (GC) as well as mass spectrometry, electrochemical sensors, and colorimetric assays.[23–27] Although these methods are well established and capable of producing reliable quantitative data, their dependence on sophisticated instrumentation, high operational costs, and time-consuming sample preparation has hindered their broad application, particularly in biological studies.[28] Fluorescence-based detection has emerged as a powerful alternative, offering rapid, highly sensitive, and minimally invasive analysis of H_2S in complex biological environments.[29–31] Unlike conventional methods, fluorescent probes enable real-time monitoring without extensive sample preparation, making them particularly suitable for *in situ* and live-cell applications. The versatility of organic fluorophores further enhances their utility; their chemical structure can be readily tailored to achieve desirable properties such as selectivity, tuneable emission wavelengths, and biocompatibility.[32–36] In cellular imaging, these probes demonstrate clear advantages, including high signal-to-noise ratios, excellent spatial resolution, and compatibility with dynamic biological systems. Over the past decade, a diverse library of fluorescent probes has been developed, each incorporating different fluorophore moieties to optimize sensitivity and selectivity toward endogenous H_2S.[37–42] Among these fluorophores, **Nap** has been especially prominent, valued for its robust photostability, ease of structural modification, and broad functional versatility in probe design.[43,44] Fluorescent sensing of H_2S has primarily evolved along two conceptual pathways. The first involves reaction-based probes, which exploit the distinct reductive properties and strong nucleophilicity of H_2S.[45–48] The second employs metal-coordination or displacement strategies, where H_2S selectively interacts with metal centers to generate a measurable signal.[49–52]

Among these, reaction-based systems have proven especially advantageous owing to their ease of synthesis, adaptability, and high degree of molecular selectivity. These probes typically rely on H_2S-triggered chemical transformations such as the reduction of functional groups (*e.g.*, nitro,[45] azide,[53] or selenoxide[54] moieties), thiolysis reactions involving dinitrophenyl ethers,[47] and various nucleophilic substitution or addition reactions (see

Sankarasekaran Shanmugaraju

Dr. Sankarasekaran Shanmugaraju received his Ph.D. in Inorganic Chemistry from the Indian Institute of Science (IISc), Bengaluru. In 2014, he joined Trinity College Dublin, Ireland, as an Irish Research Council (IRC) postdoctoral fellow. He began his independent academic career in October 2018 as an Assistant Professor in the Department of Chemistry at the Indian Institute of Technology Palakkad, where he has been serving as an Associate Professor since June 2023. His research group focuses on the design and self-assembly of novel molecular architectures, functional materials, and porous polymers for applications in emerging sustainable technologies.

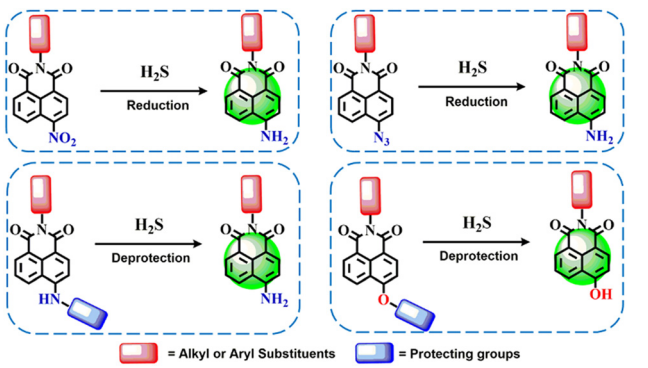

Scheme 1 Chemical transformation, such as reduction- and deprotection-based reactivity of **Nap** fluorescent sensors for H_2S detection.

Scheme 1).[55,56] By integrating these mechanisms into fluorogenic scaffolds, researchers have developed probes capable of quantifying H_2S with remarkable sensitivity. Importantly, these probes demonstrate strong discrimination of H_2S over other biologically relevant sulfur-containing compounds and general reductants, underscoring their utility in complex cellular environments.

Despite the rapid progress in the development of **Nap**-derived fluorescent probes, the literature still lacks a dedicated review that exclusively surveys their application in H_2S detection and imaging. To address this gap, the present article provides a comprehensive overview of recent advances in **Nap**-derived small-molecule chemosensors designed for fluorescence monitoring of H_2S. Particular emphasis is placed on their structural features, sensing mechanisms, detection strategies, response behaviours, and demonstrated applications. By summarizing the current progress in the field, this review aims to provide researchers with a critical perspective on existing probe designs and to lay the groundwork for developing next-generation fluorescence-based sensing platforms for H_2S detection.

2. 1,8-Naphthalimide-based fluorescent probes for H_2S

This section discusses the design, synthesis, and reactivity-based fluorescent sensing behaviour of **Nap** probes toward H_2S. For easy understanding and clarity, the **Nap** probes are categorized into three main classes based on their H_2S-triggered chemical transformations: (i) nitro group reduction, (ii) azide group reduction, and (iii) thiolysis-induced deprotection.

2.1. H_2S sensing by reduction of nitro group

The work by Montoya and Pluth represents a significant early contribution to the field of H_2S sensing using the naphthalimide system.[45] In this study, a nitro-containing naphthalimide probe **Nap-1** was designed to exploit the unique reductive chemistry of H_2S, specifically its ability to convert nitro into amine, thereby restoring fluorescence in a non-emissive nitro-naphthalimide scaffold (Fig. 1A). **Nap-1** showed significant fluorescence "turn-on" responses at λ = 542 nm after titrating with H_2S, exhibiting a 15-fold increase in fluorescence emission within 90 minutes (Fig. 1B). The detection limit was in the range of 5–10 μM. The selectivity of **Nap-1** toward H_2S was evaluated through titration experiments involving various reactive sulfur, oxygen, and nitrogen species (RSONs), each tested at 100 equivalents (Fig. 1C). For comparison, cysteine and glutathione (GSH) were examined at higher concentrations of 10 mM (2000 equivalents). Notably, **Nap-1** displayed a considerable selectivity for H_2S compared to other RSONs; however, the addition of 2000 equivalents of cysteine or GSH significantly reduced the selectivity. The biological applicability of **Nap-1** was validated using imaging tests in HeLa cells, where the probe effectively revealed the presence of intracellular H_2S (Fig. 1D).

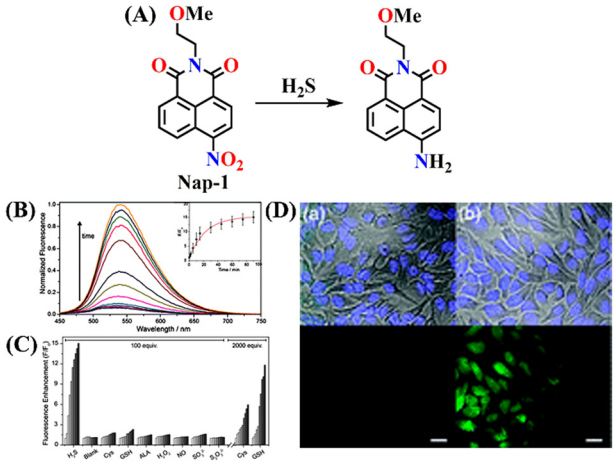

Fig. 1 (A) Chemical structure of **Nap-1** and its corresponding amino product formed upon reduction by H_2S. (B) Fluorescence "turn-on" response of **Nap-1** upon titration with H_2S (inset: time-dependent fluorescence enhancement). (C) Relative fluorescence intensity changes of **Nap-1** after treatment with various reactive species. (D) Fluorescence imaging of H_2S in HeLa cells incubated with 5 μM **Nap-1**: (a) cells treated with **Nap-1** only; (b) cells treated with **Nap-1** and H_2S. Top: DIC images with nuclear stain overlay. Bottom: fluorescence images. Scale bars = 25 μm. Reproduced with permission from ref. 45. Copyright 2012, Royal Society of Chemistry.

In 2015, Cao and co-workers reported a simple 1,8-naphthalimide fluorescence 'turn-on' probe (**Nap-2**) for the quantitative detection of H_2S, through a selective reduction of a nitro group to an amino group, which showed a strong internal charge transfer (ICT) emission at λ = 538 nm (Fig. 2A).[57] Upon exposure to H_2S in a DMSO/H_2O medium, **Nap-2** elicited up to 30-fold fluorescence

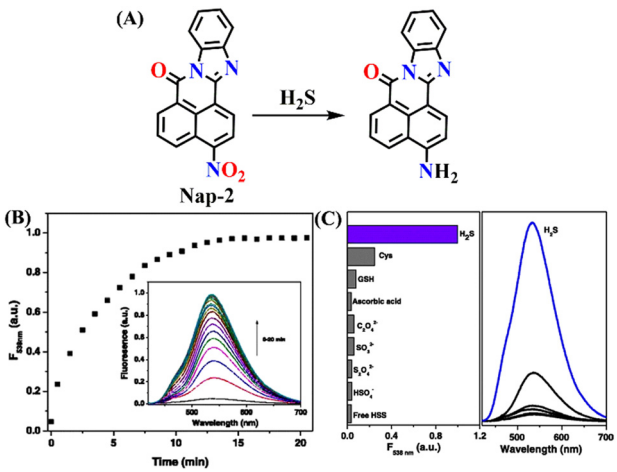

Fig. 2 (A) Chemical structure of **Nap-2** and its corresponding amino product formed upon reduction by H_2S. (B) The fluorescence enhancement observed at λ = 538 nm after incubation with H_2S (1.4×10^{-4} M, 10 equiv.) at 25 °C (λ_{ex} = 409 nm). (C) The selectivity plot demonstrates the high selectivity of **Nap-2** for H_2S over other analytes. Reproduced with permission from ref. 57. Copyright 2015, Springer.

enhancement within a short response time (~15 minutes). **Nap-2** is markedly faster than many previously reported reaction-based H_2S sensors (Fig. 2B). The probe displayed a linear fluorescence response for the 0.0 to 100 μM range, making it suitable for quantitative analysis at physiologically relevant H_2S concentrations. Selectivity tests confirmed that **Nap-2** is highly specific to H_2S compared to other common reducing agents and biothiols, with minor interference from cysteine and glutathione (Fig. 2C). The fast kinetics, strong fluorescence enhancement, and high selectivity demonstrated that **Nap-2** could serve as a robust and practical probe for biological H_2S detection.

A study by Velmathi *et al.* reported an interesting 1,8-naphthalimide-based molecular probe, **Nap-3**, which showed a rare ability to detect CN^-, Fe^{3+}, and particularly H_2S with high selectivity (Fig. 3A).[58] While CN^- and Fe^{3+} are recognized through a fluorescence relay "on–off" mechanism, H_2S was sensed *via* a chemodosimetric reduction of the nitro group to an amine, producing a distinct red colorimetric response with no fluorescence enhancement (Fig. 3B). This selectivity toward H_2S was confirmed by UV-vis absorption, potentiometric titration, and DFT studies, establishing a clear mechanistic basis for the observed color change. The appearance of a new absorption band at λ = 560 nm corroborated the formation of an amine product (Fig. 3C), while potentiometric titrations confirmed the redox interaction. The limit of detection for H_2S was determined to be 8.1 μM, a range relevant to biological systems. The probe maintained efficacy across a physiological pH range (7–11), underscoring its potential for biological applications.

In 2025, Sunil and co-workers reported a fluorene–naphthalimide hybrid (**Nap-4**) as a dual-mode probe that integrates electrochemical and fluorescence-based strategies for highly sensitive detection of H_2S.[59] The design relied on the incorporation of a nitro-naphthalimide moiety, which acts as both an electron-withdrawing and a reducible recognition unit, conjugated with a fluorene group that enhances photophysical stability. Upon reduction of the nitro group by H_2S to an amino group, significant alterations in intramolecular charge transfer occur, leading to marked changes in both the redox profile and the fluorescence response (Fig. 4). Electrochemical studies using square wave voltammetry established a detection limit as low as 12.15 nM at physiological pH, while fluorescence measurements afforded a detection limit of 14 mM. Structural and mechanistic insights were further confirmed through DFT calculations, XPS, and SEM analysis of sulfur deposition. Beyond *in vitro* sensing, the probe was successfully applied to monitor endogenous H_2S in HEK293T cells, demonstrating enhanced fluorescence under nutrient-limited conditions that stimulate autophagy, linking the probe's response to dynamic biological changes in redox homeostasis. Importantly, cytotoxicity assays confirmed good biocompatibility, supporting its applicability in live-cell imaging. This work is significant not only for achieving dual electrochemical and fluorescence detection of H_2S with high sensitivity and selectivity but also for demonstrating how molecular probe design can be extended to visualize stress-induced endogenous H_2S production, thereby offering a versatile tool for both biomedical and environmental studies.

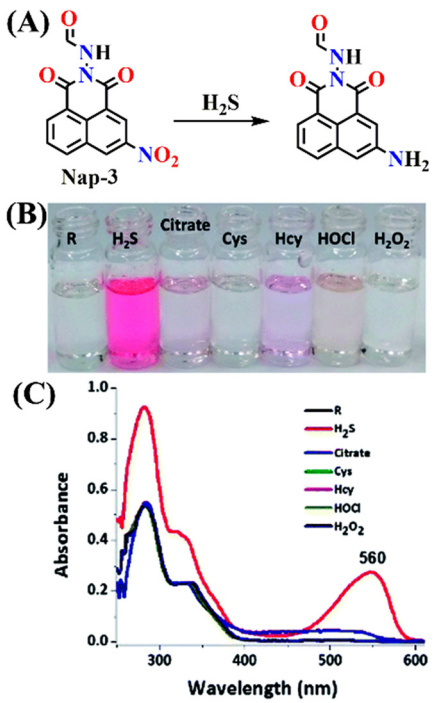

Fig. 3 (A) Chemical structure of **Nap-3** and its corresponding amino product formed upon reduction by H_2S. (B) Naked eye image of H_2S selectivity among all RSS and ROS by **Nap-3** (labelled as R) *via* colorimetric output. (C) Electronic absorption response of receptor **Nap-3** with all RSS and ROS. Reproduced with permission from ref. 58. Copyright 2020, Royal Society of Chemistry.

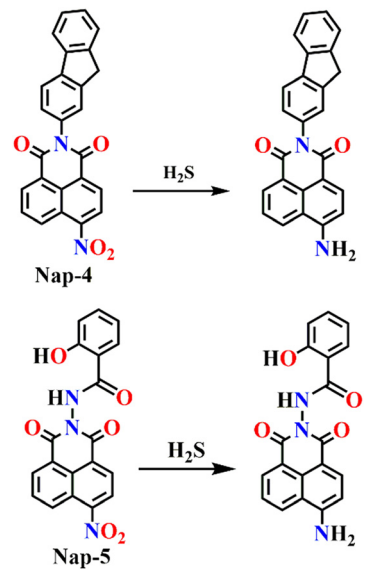

Fig. 4 Chemical structure of **Nap-4** and **Nap-5** and their corresponding amino products formed upon reduction by H_2S.

As an extension to this, the same group very recently reported a multifunctional probe, 2-hydroxy-*N*-(6-nitro-1,3-dioxo-1*H*-benzo[*de*]isoquinolin-2(3*H*)-yl)benzamide (**Nap-5**), capable of dual-mode detection of H_2S through both optical and electrochemical techniques while also enabling real-time fluorescence imaging of fungal species.[60] The probe combines a nitro-naphthalimide fluorophore with a salicyl hydrazide unit to achieve selective H_2S sensing *via* reduction of the nitro group to an amino group, resulting in distinct UV-visible and fluorescence responses (Fig. 4). In UV-visible absorption studies, **Nap-5** exhibited a characteristic band at λ = 346 nm that gradually diminished upon addition of Na_2S, accompanied by the emergence of a new absorption band at λ = 460 nm with a well-defined isosbestic point at 400 nm, confirming a clean conversion between the two species. A distinct visual colour change accompanied the reduction process, wherein the initially colourless solution gradually developed a brown tint as the concentration of Na_2S increased. Fluorescence spectroscopic titration studies further revealed a ratiometric response: the emission peak at λ = 467 nm decreased and a new band at λ = 558 nm emerged with increasing H_2S concentration, indicating the formation of the amino derivative. Time-dependent measurements showed the completion of the reaction within 20 hours, yielding a stable fluorescent product. The probe displayed strong selectivity toward H_2S over other thiol-containing species and metal ions, along with good photostability and low cytotoxicity. Based on spectroscopic analysis, the detection limit for H_2S was estimated to be 13.20 mM. Comprehensive electrochemical, spectroscopic, and theoretical studies established the reduction mechanism and pH-dependent behaviour of **Nap-5**.

2.2. H_2S sensing by reduction of the azide group

While **Nap-1** exhibited good selectivity for H_2S over reactive sulfur, oxygen, and nitrogen species (RSONs), its performance was compromised in the presence of high concentrations of biologically abundant thiols such as cysteine and glutathione (10 mM, ~2000 equivalents), which diminished its selectivity. To address this limitation, Pluth designed an azide-based probe, **Nap-6**, which exhibited a better sensing performance for H_2S detection (Fig. 5A).[45] **Nap-6** achieved a rapid and substantial 60-fold fluorescence enhancement within 45 minutes (Fig. 5B) and maintained detection limits in the low micromolar range (1–5 μM). More importantly, **Nap-6** displayed markedly higher selectivity for H_2S over cysteine and glutathione, even at millimolar concentrations, thereby overcoming a major challenge in the development of biologically relevant H_2S probes (Fig. 5C). The applicability of **Nap-6** was further demonstrated in live-cell imaging experiments in HeLa cells, where intracellular H_2S could be visualized, with **Nap-6** producing stronger and more reliable fluorescence responses (Fig. 5D). This pioneering work established the feasibility of using naphthalimide scaffolds for selective, reaction-based H_2S sensing. It highlighted how

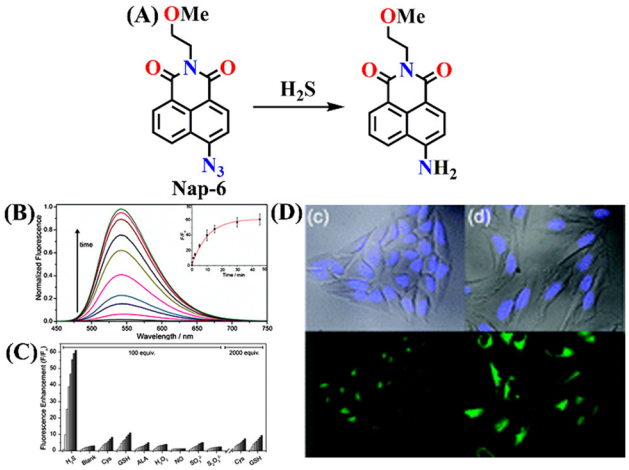

Fig. 5 (A) Chemical structure of **Nap-6** and its corresponding amino product formed upon reduction by H_2S. (B) Fluorescence "turn-on" response of **Nap-6** upon titration with H_2S (inset: time-dependent fluorescence enhancement). (C) Relative fluorescence intensity changes of **Nap-6** after treatment with various reactive species. (D) Fluorescence imaging of H_2S in HeLa cells incubated with 5 μM **Nap-6**: (c) cells treated with **Nap-6** only; (d) cells treated with **Nap-6** and H_2S. Top: DIC images with nuclear stain overlay. Bottom: fluorescence images. Scale bars = 25 μm. Reproduced with permission from ref. 45. Copyright 2012, Royal Society of Chemistry.

tuning the reducible functionality, from nitro to azide, can significantly enhance selectivity and biological utility.

Guo *et al.* reported another interesting example of a naphthalimide-based fluorescent probe (**Nap-7**) designed for

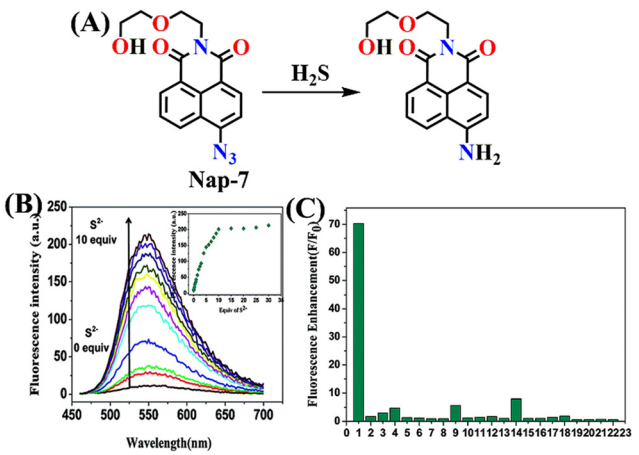

Fig. 6 (A) Structure of **Nap-7** and its amino product formed after reduction by H_2S. (B) Fluorescence spectra (λ_{ex} = 440 nm) of **Nap-7** (10 μM) with 0–100 μM Na_2S (10 equiv.) in 20 mM pH 7.4 HEPES buffer (containing 50% DMSO). The inset is the corresponding relationship between fluorescence intensity and 0–300 μM Na_2S (30 equiv.) (λ_{ex} = 440 nm, λ_{ex} = 534 nm). (C) Fluorescence response of **Nap-7** towards different analytes ((1) 100 μM Na_2S, (2) 100 μM SO_3^{2-}, (3) 100 μM $S_2O_3^{2-}$, (4) 100 μM $S_2O_4^{2-}$, (5) 1 mM SCN^-, (6) 1 mM SO_4^{2-}, (7) 1 mM Cl^-, (8) 1 mM Br^-, (9) 1 mM I^-, (10) 1 mM NO_3^-, (11) 1 mM NO_2^-, (12) 1 mM HPO_4^{2-}, (13) 1 mM HCO_3^-, (14) 1 mM ClO_3^-, (15) 1 mM OAc^-, (16) 1 mM citrate, (17) 1 mM Co^{2+}, (18) 100 mM HSO_3^-, (19) 100 mM $S_2O_7^{2-}$, (20) 1 M ClO_3^-, (21) 1 M H_2O_2, and (22) 1 M CrO_3). Reproduced with permission from ref. 61. Copyright 2014, Royal Society of Chemistry.

highly selective detection of H_2S in aqueous environments, based on an azide-to-amine reduction strategy (Fig. 6A).[61] The probe **Nap-7** was synthesized *via* a simple two-step route and functionalized with a hydroxyl diethyl ether substituent to enhance water solubility, making it suitable for environmental applications. In buffered aqueous DMSO medium, **Nap-7** exhibited weak fluorescence (Φ = 0.012), but in the presence of Na_2S, a robust fluorescence "turn-on" response was observed, with a more than 25-fold intensity increase and good linearity in the range of 0–40 μM (Fig. 6B). The detection limit was found to be as low as 0.37 μM by fluorescence measurements, and 1.4 ppb in water samples after a simple pre-treatment, highlighting its excellent sensitivity. Importantly, **Nap-7** displayed remarkable selectivity, showing negligible interference from a wide range of reactive sulfur, oxygen, and nitrogen species (RSONs), anions, cations, and ROS, even at concentrations much higher than that of H_2S (Fig. 6C). The response was also rapid, reaching completion within 15 minutes, making it suitable for practical monitoring. Application to real water samples (tap, mineral, and lake) showed excellent recoveries ranging from 94% to 108%, with low relative standard deviations, confirming the method's analytical reliability. This work not only reinforced the utility of azide-to-amine reduction chemistry for H_2S recognition but also extended the use of naphthalimide scaffolds beyond biological systems into environmental monitoring, setting a precedent for designing selective, water-compatible probes for gasotransmitter detection.

In 2016, Choi and co-workers advanced the concept of azide reduction further by reporting two naphthalimide-based probes (**Nap-8** and **Nap-9**) for H_2S detection, designed with structural variations at the N-imide site to tune the solubility and sensing performance (Fig. 7A).[62] Both probes responded selectively to H_2S by converting the azide group into an amine, restoring ICT and yielding strong fluorescence "turn-on" signals. Among the two probes, **Nap-8** exhibited much stronger sensing performance than **Nap-9**. When treated with H_2S, **Nap-8** produced nearly a 70-fold fluorescence enhancement at λ = 550 nm (Fig. 7B, inset). It also achieved a high quantum yield of 0.72 and a very low detection limit of less than 0.3 μM in PBS buffer. In addition, **Nap-8** reacted with faster kinetics compared to **Nap-9**, making it the more efficient probe. Importantly, **Nap-8** displayed excellent selectivity against other reactive species and biothiols as well as strong water solubility without the need for organic co-solvents (Fig. 7B).

The biological applicability of **Nap-8** and **Nap-9** was validated through confocal fluorescence imaging in RAW264.7 macrophage cells. Both probes were cell-permeable and minimally cytotoxic (>90% cell viability at 20 μM after 24 h). Cells treated with **Nap-8** alone showed negligible background fluorescence, but a bright green emission was observed after exposure to NaHS, with **Nap-8** showing much stronger intensity due to its enhanced solubility and cellular retention (Fig. 7C). Extending to *in vivo* models, **Nap-8** successfully visualized endogenous H_2S in zebrafish embryos, with signals localized in the yolk, brain, and spinal cord, and its specificity confirmed by aminooxyacetic acid (AOAA) inhibition experiments. Overall, this study demonstrates how modifying the structure of naphthalimide scaffolds can significantly enhance solubility and sensitivity, with **Nap-8** serving as a powerful probe for both cellular and whole-organism imaging of H_2S.

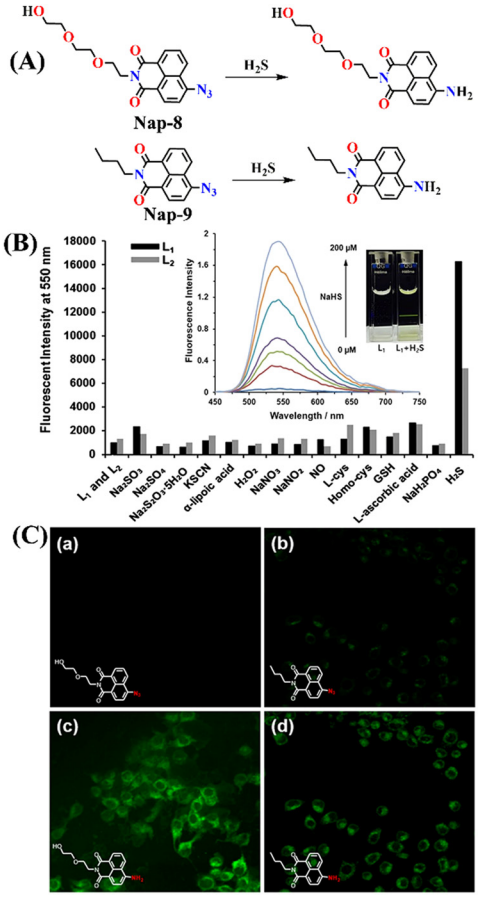

Fig. 7 (A) Structure of **Nap-8** and **Nap-9** and their amino product formed after reduction by H_2S. (B) Fluorescence responses of **Nap-8** and **Nap-9** (10 μM) toward various analytes and NaHS (100 μM) in PBS buffer (pH 7.4) at 37 °C for 60 min. Excitation at 435 nm (inset: time-dependent fluorescence spectra of **Nap-8** (10 μM) with NaHS in PBS (pH 7.4) at 37 °C for 30 min, and visual color changes observed). (C) Fluorescence images of exogenous H_2S in living RAW264.7 cells incubated with **Nap-8** and **Nap-9**. Cells were incubated with only 5 μM probes for 30 min (a and b) and with probes for 30 min and then 200 μM NaHS for 5 min (c and d), under λ = 488 nm excitation. Images were acquired with emission channels of λ = 505–605 nm (green). Reproduced with permission from ref. 62. Copyright 2016, Nature Portfolio.

In 2020, Lin *et al.* reported an ICT-based naphthalimide fluorescent probe (**Nap-10**) incorporating a bridging Si–O–Si unit for the selective visualization of H_2S in lipid droplets of living cells (Fig. 8A).[63] The probe design employs an azide-functionalized 1,8-naphthalimide as the H_2S-responsive unit, wherein H_2S-triggered reduction of the azide to the corresponding amine converts an electron-withdrawing group into a strong electron donor. This transformation effectively

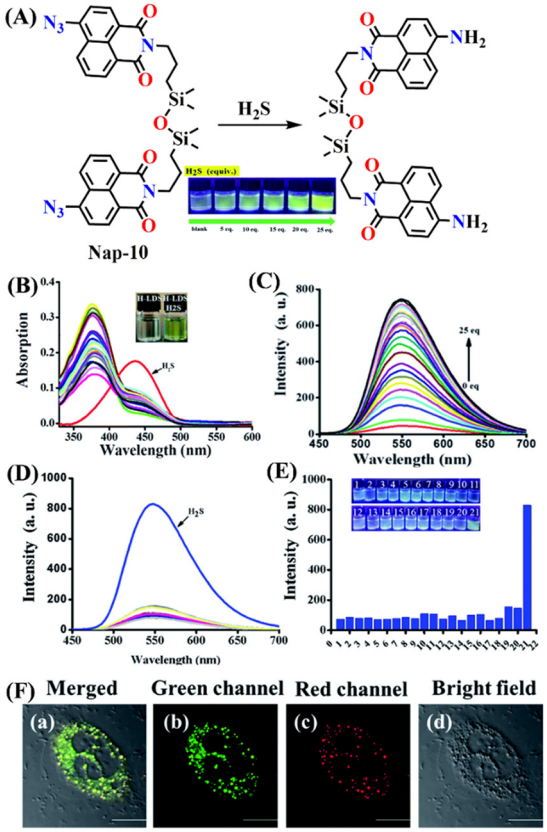

Fig. 8 (A) Structure of **Nap-10** and its amino product formed after reduction by H_2S (photographs imaged at different equivalents of H_2S under light illumination). (B) The absorption spectra of **Nap-10** in the presence of different analytes and H_2S (color of the sensor before and after H_2S addition). (C) Fluorescence spectra of **Nap-10** in aqueous solution upon addition of different concentrations of H_2S. (D) Fluorescence response of **Nap-10** towards different analytes in aqueous solution. (E) Fluorescence intensity monitored at λ = 550 nm of **Nap-10** in the presence of different ions ((1) **Nap-10**, (2) Cys, (3) D-Cys, (4) $EtOONH_4$, (5) Glu, (6) Gly, (7) KNO_3, (8) $NaNO_2$, (9) $Na_2S_2O_3$, (10) NaBr, (11) NaCl, (12) NaClO, (13) NaCNS, (14) NaF, (15) $NaHCO_3$, (16) NaI, (17) Na_2SO_3, (18) Na_2SO_4, (19) Na_2CO_3, (20) $Na_2S_2O_4$, and (21) H_2S) in aqueous solution, λ_{ex} = 405 nm. (F) Co-localization of **Nap-10** and Nile Red neutral lipid stains in HeLa cells, (a) merged image of (b)–(d); (b) green channel λ_{ex} = 405 nm, collected 500–550 nm; (c) Nile Red neutral lipid stains, λ_{ex} = 561 nm, collected 570–620 nm; (d) bright field. Reproduced with permission from ref. 63. Copyright 2020, Royal Society of Chemistry.

activates the ICT process, resulting in a prominent fluorescence turn-on response. The introduction of an organosilicone (Si–O–Si) linker not only improves biocompatibility but also facilitates preferential localization in lipid droplets, thereby enabling subcellularly resolved H_2S imaging. Probe **Nap-10** exhibits a characteristic ICT-driven spectral response toward H_2S. In the absorption spectra, the addition of H_2S induces a noticeable red shift accompanied by the appearance of a new absorption band around λ = 440 nm, consistent with enhanced ICT following azide-to-amine reduction (Fig. 8B). Correspondingly, the fluorescence spectra display a strong turn-on emission centered at approximately λ = 550 nm, with the emission intensity increasing linearly over a relevant H_2S concentration range and reaching saturation within minutes, indicative of rapid reaction kinetics (Fig. 8C). Notably, the probe shows minimal interference from common biological anions, thiols, and metal ions, underscoring its high selectivity for H_2S (Fig. 8D). Beyond solution studies, probe **Nap-10** demonstrated favorable biological performance, including low cytotoxicity, good photostability, and efficient cellular uptake. Importantly, the presence of the Si–O–Si linker confers pronounced lipid droplet targeting, as evidenced by strong co-localization with Nile Red in HeLa cells (Fig. 8E).

Iyer and co-workers reported a novel probe (**Nap-11**) constructed by linking two azide-functionalized naphthalimide units *via* an ethylene bridge bearing two cyano substituents (Fig. 9A).[64] **Nap-11** utilizes the reduction of an azide group to an amine for highly selective "turn-on" detection of hydrogen sulfide in both environmental and biological samples. The probe exhibited weak background

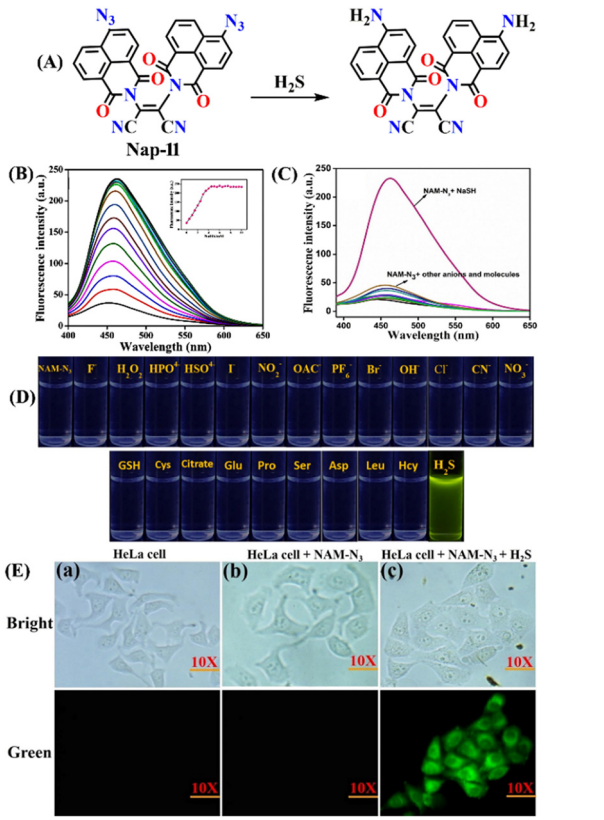

Fig. 9 (A) Structure of **Nap-11** and its amino product formed after reduction by H_2S. (B) Change in fluorescence intensity of **Nap-11** (2 μM) over the incremental addition of H_2S (up to 5 equiv.; inset: plot of fluorescence intensity against the concentration of H_2S). (C) Fluorescence spectra of probe **Nap-11** (labelled as NAM-N_3) (2 μM) upon addition of various analytes (10 equiv.). (D) Photographs of **Nap-11** in the presence of various anions and H_2S under a UV lamp at 365 nm. (E) Bright-field and fluorescence images of HeLa cells treated with **Nap-11** and H_2S; (a) HeLa cells alone, (b) HeLa cells treated only with **Nap-11** (labelled as NAM-N_3), (c) HeLa cells treated with **Nap-11** (labelled as NAM-N_3) and H_2S. The scale bar is 50 μm. Reproduced with permission from ref. 64. Copyright 2021, Elsevier.

emission due to PET quenching, but upon exposure to H_2S, a strong green fluorescence at λ = 452 nm was rapidly restored with significant emission enhancement as the azide was reduced to an electron-donating amine (Fig. 9B). **Nap-11** demonstrated an excellent selectivity over other anions, reactive oxygen/nitrogen species, and biothiols (Fig. 9C), and showed a linear response up to 5 μM H_2S with a low detection limit of 1.5 μM. Selective sensing of H_2S was also reflected by a marked color change from colourless to bright green emission (Fig. 9D). The response was fast, reaching completion within 2 seconds, and fluorescence intensity remained stable across a broad pH range (4–10), highlighting the probe's suitability for real-time monitoring. Quantum yield analysis further revealed a ~5.3-fold increase upon reduction, confirming the efficiency of the sensing mechanism. Practical applicability was validated by detecting H_2S in environmental matrices (tap water, lake water, well water, beer, and red wine), with recovery rates between 87% and 94% and RSD values below 1.5%, demonstrating analytical reliability. Moreover, **Nap-11** successfully penetrated HeLa cells and enabled fluorescence bioimaging of intracellular H_2S, showing strong green fluorescence only after sulfide treatment, with negligible background in controls (Fig. 9E). Importantly, compared to earlier multistep and slower systems, **Nap-11** offers a simple synthetic route, ultrafast response, and practical dual applicability, reinforcing the value of azide-to-amine chemistry in the ongoing development of naphthalimide-based H_2S sensors.

Later, the same group developed another probe, **Nap-12**, incorporating a pyridylmethyl substituent at the imide site of the naphthalimide ring based on the same principles, for the selective detection of H_2S in aqueous and biological samples (Fig. 10A).[65] Spectroscopic analysis of **Nap-12** showed a distinct absorption shift from λ = 365 to 416 nm with a well-defined isosbestic point at λ = 391 nm. This spectral change was accompanied by a visible transition in solution color, from colourless to yellow, enabling both straightforward colorimetric readout and fluorescence-based sensing. Upon reduction by H_2S, the probe displayed a pronounced emission at λ = 459 nm with an approximately 5.3-fold enhancement in quantum yield (Fig. 10C). It showed a linear response in the 0–10 μM range, a low detection limit of 1.2 μM, and a rapid response time of just 8–10 seconds; outperforming many previously reported naphthalimide-based sensors. The selectivity was excellent, with negligible interference from a wide range of competing anions, ROS/RNS, or biothiols, and the fluorescence signal remained stable under physiological pH conditions (7–12) (Fig. 10B). For practical demonstration, **Nap-12** was tested in diverse real-world matrices, including tap water, lake water, well water, beer, and red wine, where it delivered recoveries of 89–97% with relative standard deviations under 1.6%. In addition, simple test strips coated with the probe showed a clear visual change from colorless to green in the presence of H_2S, highlighting its potential for portable and on-site applications (Fig. 10D). Biological imaging experiments

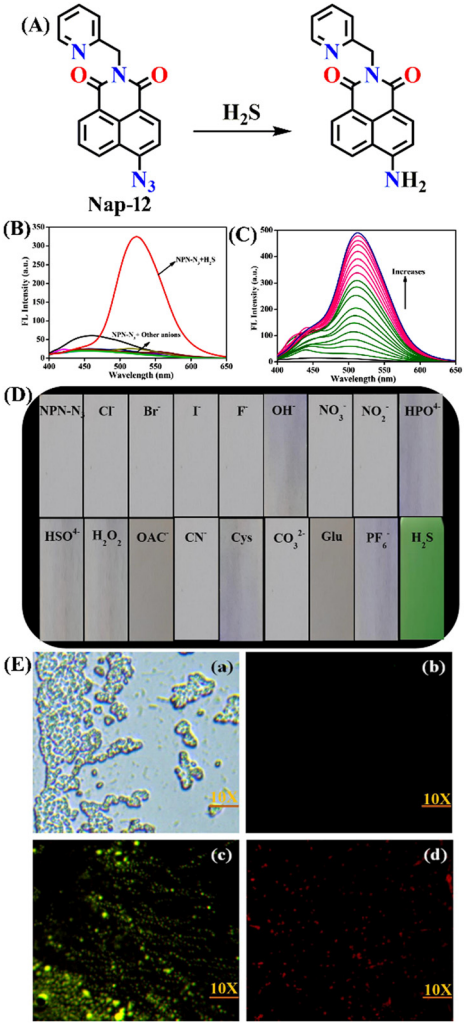

Fig. 10 (A) Structure of **Nap-12** and its amino product formed after reduction by H_2S. (B) Change in fluorescence intensity of **Nap-12** (20 μM) in the presence of various analytes and (C) fluorescence changes on the incremental addition of H_2S (0 and 80 μM). (D) Photograph showing fluorescence color change of **Nap-12** (2×10^{-5} M) coated test paper strips after treating with various anions and small molecules. (E) (a) Fluorescence bioimages of *E. coli* bacterial cells alone, (b) *E. coli* cells treated with **Nap-12**, (c) *E. coli* cells treated with **Nap-12** and H_2S using the blue channel. (d) *E. coli* cells were treated with **Nap-12** in the presence of H_2S ion using the green channel. Reproduced with permission from ref. 65. Copyright 2022, Elsevier.

further confirmed its utility: in *E. coli* cells, **Nap-12** readily penetrated and produced bright fluorescence signals upon H_2S exposure, enabling clear visualization of intracellular sulphide (Fig. 10E).

Yan and co-workers developed another simple naphthalimide-based fluorescent probe (**Nap-13**) for H_2S detection (Fig. 11A).[66] The probe was synthesized in just two steps from readily available precursors, making it more cost-effective compared to many previously reported systems, and its structure and sensing mechanism were confirmed through NMR, IR, ESI-MS, and theoretical calculations. In its azide form, probe **Nap-13** was essentially non-fluorescent; however, upon exposure to H_2S, it displayed a pronounced

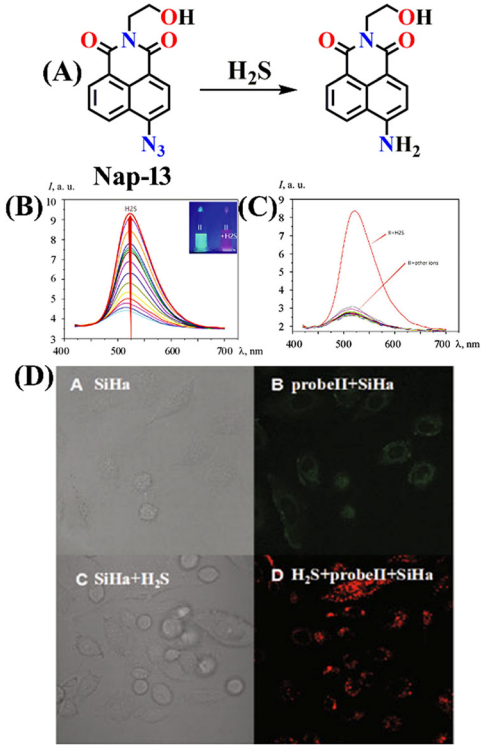

Fig. 11 (A) Structure of **Nap-13** and its amino product formed after reduction by H_2S. (B) Fluorescence spectral changes of **Nap-13** (4 μM) upon addition of Na_2S (0.0–0.70 μM) in DMSO at room temperature (inset: the visible fluorescence changes upon UV irradiation). (C) Fluorescence response of **Nap-12** upon the addition of several ions in DMSO. (D) Bright-field and fluorescence images of SiHa cells treated with **Nap-13** and H_2S. Reproduced with permission from ref. 66. Copyright 2022, Springer.

fluorescence enhancement with a strong red emission centered at λ = 510 nm (Fig. 11B) and a distinct color change under UV light in DMSO, enabling both visual and spectroscopic detection (Fig. 11B, inset). Sensitivity studies demonstrated a detection limit as low as 1×10^{-7} M. Selectivity tests revealed negligible interference from common competing species, including cations, anions, reactive sulfur and oxygen species, and biothiols such as cysteine and glutathione, indicating the probe's robustness in complex environments (Fig. 11C). Importantly, the probe was effectively applied in biological imaging. Confocal microscopy in SiHa cells revealed that the probe is cell-permeable and produces strong intracellular fluorescence upon exposure to H_2S (Fig. 11D). Moreover, it exhibited low cytotoxicity, maintaining over 80% cell viability even at concentrations up to 60 μM, underscoring its excellent biocompatibility. These results position probe **Nap-13** as a versatile and practical addition to the family of azide-functionalized naphthalimide sensors for H_2S detection and imaging.

Wang and co-workers systematically advanced naphthalimide-based H_2S probes by progressing from a single ICT-regulated design to a synergistic ICT-PET dual-controlled strategy, thereby significantly enhancing sensitivity and biological imaging performance. In their earlier study (reported in 2020),[67] an azide-functionalized naphthalimide probe (**Nap-14**) displayed typical ICT-dominated behavior, wherein H_2S-induced azide-to-amine conversion produced a red shift in the absorption spectrum along with a pronounced fluorescence turn-on in the green region, enabling rapid and selective H_2S detection under pH-controlled conditions (Fig. 12). Building on this design, a subsequent probe (**Nap-15**) was developed by introducing a PET-active *p*-hydroxyphenyl unit, which imposed dual quenching (ICT + PET) in the ground state and resulted in an exceptionally low background fluorescence (Fig. 12).[68] Upon exposure to H_2S or visible-light irradiation, azide reduction effectively suppressed the PET process while simultaneously activating ICT, leading to a strong fluorescence enhancement of approximately 17-fold and a markedly improved detection limit of 0.085 μM, representing an order-of-magnitude improvement over the single ICT-based probe. Spectral studies revealed that both probes (**Nap-14** and **Nap-15**) exhibit red-shifted absorption bands in the range of ~430–460 nm and turn-on emission centered at ~520–540 nm, consistent with a common ICT-driven signaling mechanism. Importantly, the ICT-PET dual-regulated probe **Nap-15** enabled spatiotemporal control over fluorescence activation and facilitated high-contrast imaging of exogenous H_2S in living HeLa cells, characterized by an excellent signal-to-noise ratio and minimal background interference. Collectively, these results underscore a clear design evolution in which the rational integration of multiple photophysical quenching pathways substantially improves H_2S sensing sensitivity and broadens applicability toward precise and photoactivatable cellular imaging.

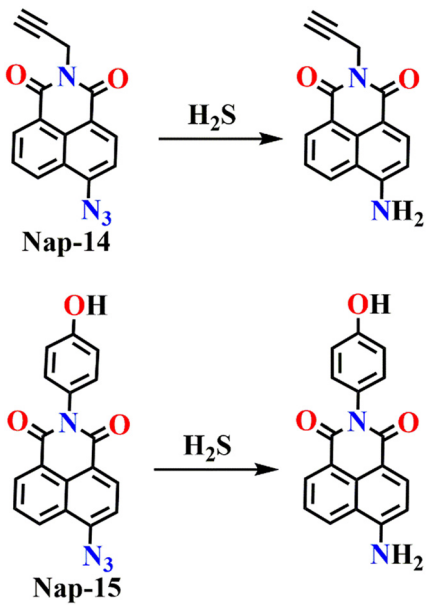

Fig. 12 Structures of probe **Nap-14** and **Nap-15** and their amino product formed after reduction by H_2S.

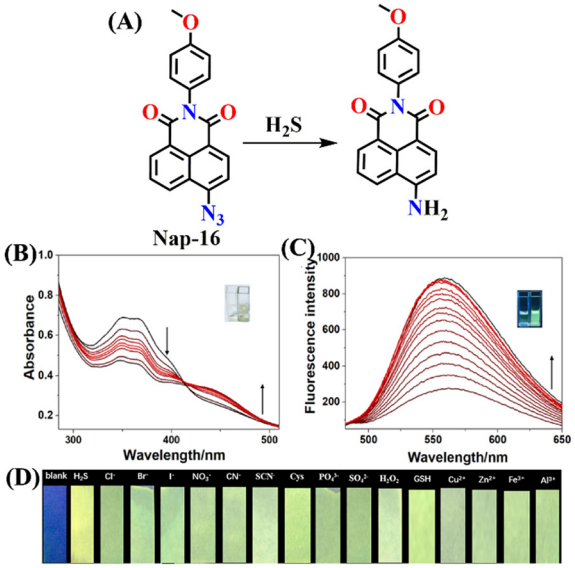

Fig. 13 (A) Structure of **Nap-16** and its amino product formed after reduction by H_2S. (B) The absorption and (C) fluorescence emission spectra of **Nap-16** in the presence of increasing concentrations of H_2S (inset: color changes observed). (D) Photograph of the luminescent test paper exposed to various anions imaged under a UV lamp. Reproduced with permission from ref. 69. Copyright 2020, Elsevier.

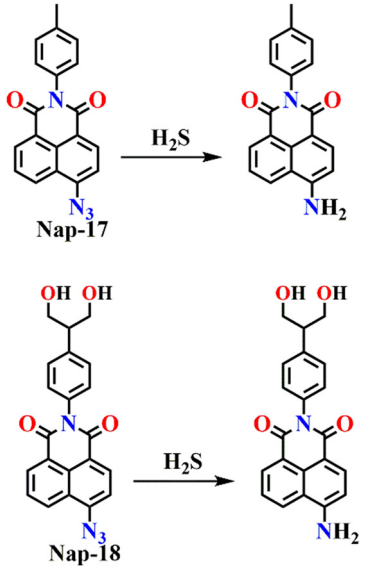

Fig. 14 Structures of probe **Nap-17** and **Nap-18** and their amino product formed after reduction by H_2S.

Zhang and co-workers reported another simple azide-functionalized fluorescent probe (**Nap-16**), structurally closely related to probe **Nap-15**, that operates *via* the selective H_2S-mediated reduction of an aryl azide to the corresponding amine.[69] In its native azide form, probe **Nap-16** is weakly emissive; however, exposure to H_2S induces the emergence of a new absorption band in the visible region along with a pronounced fluorescence turn-on in the green region (Fig. 13A). The fluorescence intensity increases in a concentration-dependent manner, delivering a low detection limit of 17.4 nM and a rapid response time within minutes. The probe demonstrates high selectivity for H_2S over common anions, biothiols, and reactive oxygen and sulfur species across a broad pH range. Biological studies revealed low cytotoxicity and efficient cellular uptake, enabling successful fluorescence imaging of exogenous H_2S in living cells. Notably, the applicability of probe 4 was further extended to food safety monitoring, where it facilitated the visual detection of H_2S released during food spoilage through observable fluorescence changes in real samples, such as red wine. Collectively, these findings illustrate that azide-reduction-based fluorescent probes offer reliable spectroscopic responses while being readily adaptable to both bioimaging and practical food-quality assessment.

In 2024, Széchenyi *et al.* reported a new azide-functionalized naphthalimide probe (**Nap-17**) for the highly sensitive detection of H_2S in human serum (Fig. 14).[70] The probe combined a 1,8-naphthalimide fluorophore with a *p*-toluidine substituent at the imide position, and an azide group served as the H_2S-responsive recognition site. This modification enhanced the photophysical properties of the scaffold, improving fluorescence output and stability under physiological conditions. The probe itself was weakly emissive, but in the presence of H_2S it underwent selective azide-to-amine reduction, leading to a pronounced "turn-on" fluorescence at λ = 520 nm. Spectral studies confirmed an excellent linear correlation between fluorescence intensity and H_2S concentration in the low micromolar range, and the detection limit was calculated to be 0.085 μM, which is lower than that of many earlier naphthalimide-based systems. Selectivity tests demonstrated that the probe responded exclusively to H_2S even in the presence of other biologically abundant anions and reactive sulfur species, underscoring the specificity of the azide reduction pathway. Practical validation was performed in human serum, where spiking experiments with 5–20 μM H_2S yielded recoveries of 95–109% and low relative standard deviations, confirming the probe's analytical reliability in complex biological environments. Importantly, the endogenous H_2S concentration in a real serum sample was quantified at 17.2 μM, consistent with physiologically reported levels, highlighting the probe's biomedical relevance. The requirement of two equivalents of H_2S for complete reduction of the azide moiety was also experimentally verified, aligning with the known mechanistic pathway.

Very recently, the same group reported another interesting serinol-modified 1,8-naphthalimide fluorescent probe, **Nap-18**, for the selective detection of H_2S in human serum and in samples from hypertensive patients (Fig. 14).[71] The probe incorporates an azide group as the H_2S-reactive site, which undergoes reduction to an amine upon exposure to H_2S, giving distinct optical responses. UV-visible spectroscopy exhibited the disappearance of the characteristic absorption band of the azide precursor and the emergence of new features consistent with the formation of the reduced amino-

naphthalimide derivative. Fluorescence spectroscopy revealed a pronounced enhancement in emission intensity at λ = 520 nm upon treatment with Na_2S, attributed to the ICT transition. The fluorescence intensity increased with H_2S concentration (5–20 μM) and reached a plateau after about 20 minutes of incubation at pH 7.4, within physiological range. The limit of detection was calculated to be 0.16 μM. The probe exhibited excellent selectivity toward H_2S over other biologically relevant thiols (Cys, GSH) and oxidative species. Quantitative analysis of human serum using **Nap-18** yielded an H_2S concentration of 17.98 μM, which correlated well with the value obtained by the standard methylene-blue UV-vis method (17.32 μM). Furthermore, significantly lower H_2S levels were detected in hypertensive patient samples, indicating the probe's potential for biomedical and clinical diagnostics.

The design of H_2S sensing probes has garnered significant interest, even within the computational domain. Haixiang He and colleagues employed density functional theory (DFT) and time-dependent DFT (TD-DFT) calculations, incorporating Grimme's D3 dispersion corrections and solvent modeling, to clarify the mechanisms of excited-state relaxation and fluorescence quenching of two 1,8-naphthalimide-based fluorescent probes (**Nap-19** and **Nap-20**) for H_2S detection (Fig. 15).[72] The authors revealed that fluorescence quenching arises from a strong coupling between the locally excited (LE) state and a closely lying dark charge-transfer (CT) state, with the system favoring non-radiative decay *via* a minimum energy conical intersection (MECI) leading to a distorted naphthalimide structure. Structural analyses demonstrate how long-chain N-substituents influence geometrical distortions and electronic distributions that facilitate the decay pathway. Upon reacting with H_2S, the resulting product molecules exhibit an increased energy gap between the LE and the CT states, losing the accessible MECI, thereby favoring radiative relaxation and producing strong fluorescence, in line with experimental results. The study further validated theoretical absorption and emission spectra alongside quantum yield calculations against experimental data, reinforcing the mechanistic insights. This work highlighted the critical role of MECIs in modulating probe fluorescence and underscores how computational insights can guide the rational design of enhanced fluorescent probes for biological gas sensing, offering a valuable framework for interpreting photophysical behaviours in related systems.

2.3. H_2S sensing by deprotection – thiolysis

Naphthalimide derivatives are well known for their strong fluorescence, which arises from an internal charge transfer (ICT) transition between an electron-donating substituent (such as an amine or hydroxyl group) on the naphthalene ring and the imide moiety. When the electron-donating ability of such substituents is suppressed through protective modification, the ICT process is attenuated or completely blocked. However, upon H_2S-triggered deprotection, the free hydroxyl/amine group is restored, thereby re-establishing the ICT pathway and producing a significant fluorescence enhancement. This thiolysis-based strategy has been applied

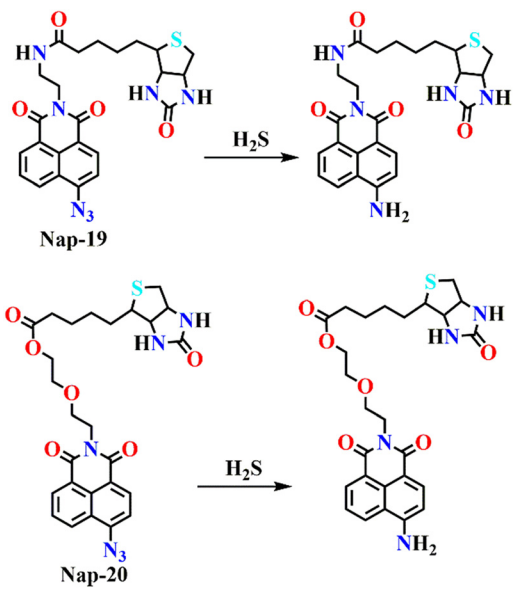

Fig. 15 Structure of **Nap-19** and **Nap-20** and their amino product formed after reduction by H_2S.

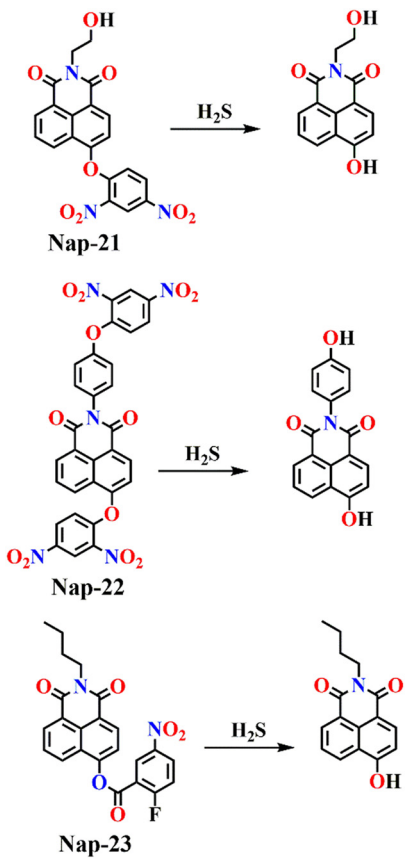

Fig. 16 Structure of **Nap-21**, **Nap-22**, and **Nap-23** and their hydroxyl product formed after thiolysis by H_2S.

in the design of several H_2S-responsive naphthalimide probes.

In 2019, Hongmei and co-workers were the first to report naphthalimide sensors that explicitly utilized this protection–deprotection approach for selective H_2S detection.[73] They developed two 1,8-naphthalimide-based fluorescent probes (**Nap-21** and **Nap-22**) for the selective detection of H_2S (Fig. 16). By combining 4-hydroxy-1,8-naphthalimide as the fluorophore with 2,4-dinitrophenyl ether as the H_2S-responsive site, they achieved a photoinduced electron transfer (PET)-based sensing system. Upon addition of H_2S, the probes displayed a distinct color change from colorless to yellow, accompanied by a large red shift in absorption (>100 nm) and more than 30-fold enhancement of yellow fluorescence emission near λ = 548–549 nm, enabling both fluorometric and naked-eye detection. Notably, the dual-site probe **Nap-22** provided a broader linear detection range (0–40 μM) compared to the single-site analogue **Nap-21** (0–30 μM), enabling more reliable quantification at higher H_2S levels. The probes demonstrated good selectivity against common interfering species and maintained functionality across biologically relevant pH ranges (5–8). Mechanistic investigations, supported by NMR and TD-DFT calculations, confirmed that thiolysis of the 2,4-dinitrophenyl ether moiety triggers the fluorescence turn-on response. Importantly, practical tests in tap water and rainwater validated their potential for environmental monitoring applications.

Based on the same strategy, S. Hu *et al.* designed a novel two-photon fluorescent probe (**Nap-23**) from 4-hydroxy-1,8-naphthalimide, using 2-fluoro-5-nitrobenzoic ester as a protection group (Fig. 16).[74] They have explored the ability of the designed two-photon probe for quantitatively detecting hydrogen polysulfides (H_2S_n, $n > 1$), and it exhibited selectivity towards H_2S_n over other reactive sulfur species (RSS), especially H_2S and biothiols. The probe is based on a 4-hydroxy-1,8-naphthalimide fluorophore in a donor–π–acceptor framework, with fluorescence initially quenched by a 2-fluoro-5-nitrobenzoic ester group. Upon reaction with H_2S_n, thiolysis removes this protective group, restoring the ICT process and producing a strong "turn-on" fluorescence response. **Nap-23** exhibited an over 80-fold fluorescence enhancement at 550 nm, and a detection limit as low as 33 nM. A key strength of this study is the application of two-photon excitation (λ = 820 nm), which provided deeper tissue penetration and high-resolution imaging compared to traditional one-photon probes. The probe was successfully used for fluorescence imaging of H_2S_n in live HeLa cells, demonstrating low cytotoxicity and good cell permeability. The fluorescence was stable across a biologically relevant pH range (4–8), further supporting its suitability for cellular applications.

Xu *et al.* developed a PET-regulated naphthalimide-based turn-on fluorescent probe (**Nap-24**) for the detection of H_2S and biothiols, in which a 2,4-dinitrobenzenesulfonyl (DNBS) group functions simultaneously as the recognition unit and a strong electron acceptor (Fig. 17A).[75] In the absence of

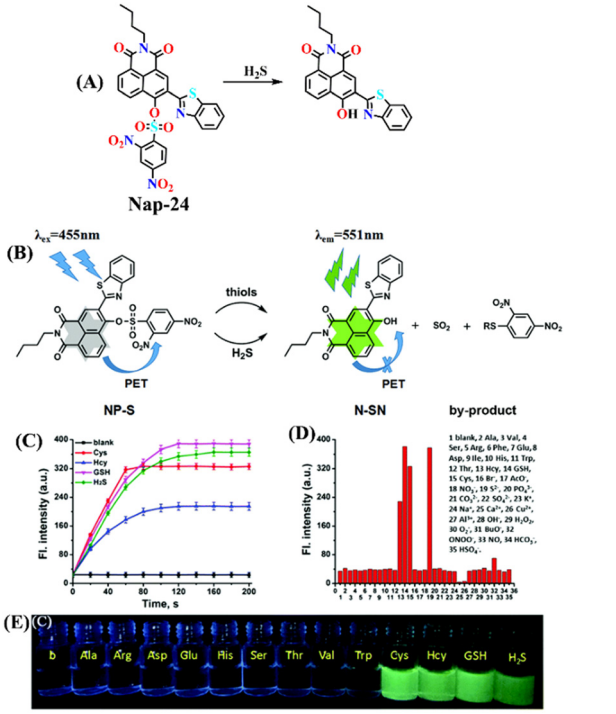

Fig. 17 (A) Structure of **Nap-24** and its product formed after reaction with H_2S. (B) The proposed sensing mechanism for the detection of H_2S. (C) Time (0 to 200 s) *vs.* fluorescence intensity (I_{551}) curves of probe **Nap-24** in the presence of various thiols and H_2S in aqueous solution. (D) The fluorescence intensities (I_{551}) of **Nap-24** mixed with various interferents in aqueous solution. (E) The ultraviolet light image of **Nap-24** with the detection target and interfering amino acids. Reproduced with permission from ref. 75. Copyright 2019, Royal Society of Chemistry.

target analytes, the excited-state fluorescence of the naphthalimide–benzothiazole fluorophore is efficiently quenched through PET to the DNBS moiety, resulting in an almost non-emissive background. Upon exposure to H_2S, cleavage of the DNBS group effectively inhibits the PET process and restores the intrinsic emission of the naphthalimide core, giving rise to a pronounced fluorescence turn-on centered at approximately λ = 551 nm, along with intensified absorption bands around λ = 385 and 470 nm (Fig. 17B). Probe **Nap-24** exhibits fast response kinetics (≤200 s), high sensitivity with a submicromolar detection limit for H_2S, and good selectivity over common amino acids and reactive species across a physiologically relevant pH window (Fig. 17C–E). Beyond solution-phase sensing, the probe shows excellent biocompatibility and robust performance in complex biological environments, enabling both one- and two-photon fluorescence imaging of H_2S/thiols in living HeLa cells, deep mouse liver tissues, and zebrafish. The large two-photon absorption cross section and effective tissue penetration underscore the potential of PET-based naphthalimide probes for *in vivo* visualization of reactive sulfur species, although discrimination between H_2S and endogenous thiols remains an inherent limitation of DNBS-based sensing strategies.

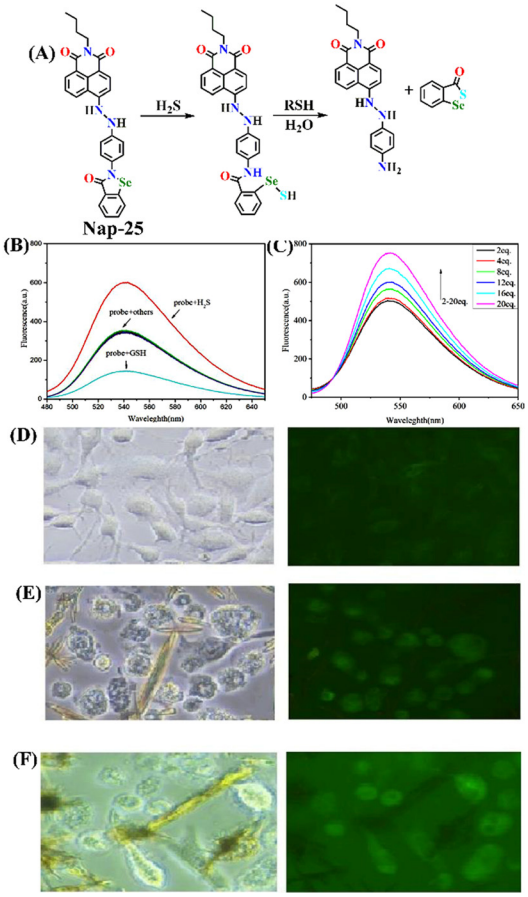

Fig. 18 (A) The proposed reactivity-based sensing mechanism for the binding of **Nap-25** with H_2S. (B) The extent of changes in fluorescence emission for **Nap-25** after adding various analytes. (C) Fluorescence spectra of probe **Nap-25** (10 μM) in a mixture of PBS buffer (pH = 7.4) and DMSO (10%) upon the gradual mixing of H_2S with different concentrations. (D–F) Fluorescence imaging of cells incubated with **Nap-25** and varied concentrations of Na_2S. From (D) to (F), the concentrations of Na_2S are 0, 50, and 100 μM, respectively. Reproduced with permission from ref. 76. Copyright 2022, Elsevier.

Liu and co-workers later reported a 1,8-naphthalimide–ebselen fluorescent probe (**Nap-25**) for highly selective and sensitive detection of H_2S in both biological and environmental samples.[76] The probe displayed a rapid turn-on fluorescence response with a high quantum yield (Φ = 0.5932), a large Stokes shift of 125 nm, and excellent stability over a broad pH range (5–11), making it well-suited for physiological conditions. Mechanistic investigations using NMR titration and HRMS established that the sensing process involves H_2S-mediated nucleophilic cleavage of the Se–N bond in the ebselen moiety, generating an electron-donating amino group at the 4-position of the 1,8-naphthalimide core (Fig. 18A). This transformation enhances intramolecular charge transfer (ICT), producing a pronounced fluorescence increase that directly links the molecular design to its sensing function. Probe **Nap-25** demonstrated excellent selectivity against common ions, amino acids, and biomolecules, with competitive assays confirming that its response to H_2S remains unaffected by high concentrations of potential interferents such as glutathione (GSH) (Fig. 18B). It featured a low detection limit of 0.129 μM and a fast response time (<90 s), making it suitable for real-time monitoring. In biological studies, **Nap-25** exhibited low cytotoxicity in GBC-SD cells and enabled clear confocal imaging of exogenous H_2S, with fluorescence intensity increasing proportionally to H_2S concentration (Fig. 18C–F). Beyond cellular imaging, **Nap-25** was also validated for environmental monitoring, where quantitative detection in tap, river, and seawater samples yielded high recovery rates (92–102%), highlighting its robustness and broad applicability.

In 2024, Huang *et al.* reported a detailed theoretical study on three ratiometric 1,8-naphthalimide fluorescent probes (**Nap-26**, **Nap-27**, and **Nap-28**) for H_2S detection using DFT and TDDFT methods (see Fig. 19A).[77] The theoretical calculations showed that while substituent modifications have minimal effect on the core 1,8-naphthalimide skeleton, they significantly influence local bond angles, dihedral angles, and electronic properties, leading to redshifts in absorption and emission spectra when electron-withdrawing strength at C4 or electron-donating ability at the imide nitrogen increases. Importantly, the study suggested that for one probe (**Nap-26**), the true sensing species is a deprotonated product rather than the neutral hydroxylated form proposed experimentally, offering new mechanistic insight. Frontier molecular orbital analysis confirmed the

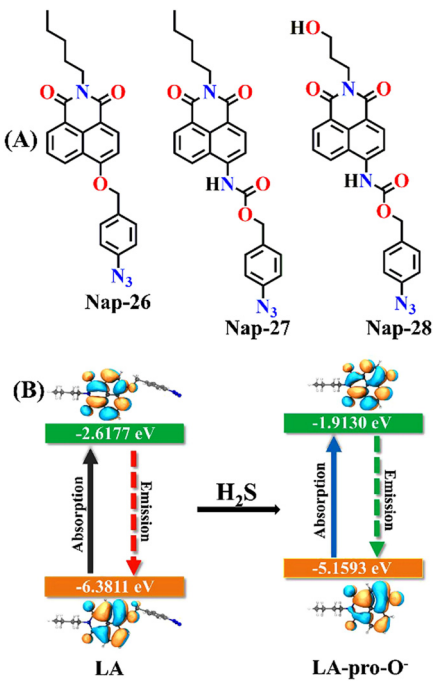

Fig. 19 (A) Molecular structures of probes **Nap-26**, **Nap-27**, and **Nap-28**. (B) Frontier molecular orbital distributions and corresponding energies of probe **Nap-26** (labelled as LA) and its product (labelled as LA-pro-O^-). Reproduced with permission from ref. 77. Copyright 2025, Springer.

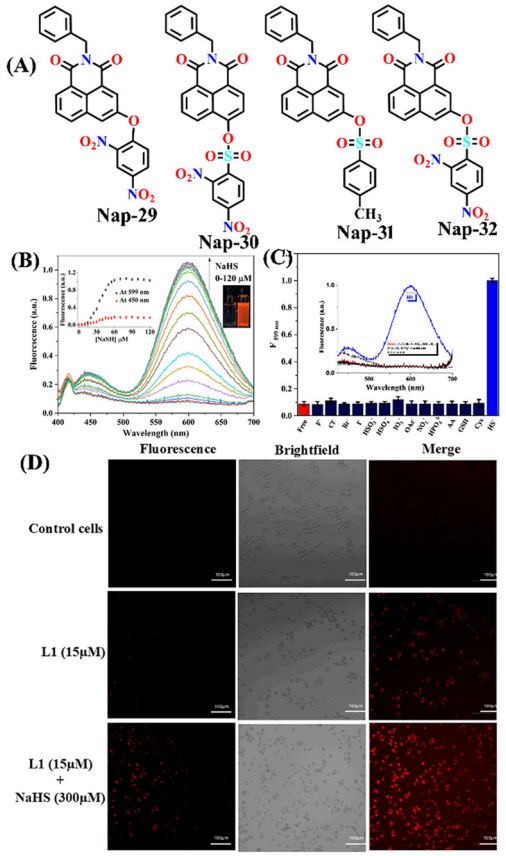

Fig. 20 (A) Molecular structures of probes **Nap-29**, **Nap-30**, **Nap-31**, and **Nap-32**. (B) Fluorescence emission spectra of **Nap-29** (10 μM) upon titration with increasing concentrations of NaHS (0–120 μM) in DMSO-phosphate buffer (0.01 M) at pH 7.4 (3 : 7, v/v) at room temperature (λ_{ex} = 351 nm) (inset: color changes observed before and after the addition of NaHS). (C) Fluorescence response of **Nap-29** (10 μM) upon addition of various analytes. (D) Confocal images of MDA-MB-231: (top row) untreated control cells, (middle row) cells treated with only 15 μM **Nap-29** probe, (bottom row) cells pretreated with 300 μM NaHS followed by treatment with 15 μM **Nap-29** probe. Reproduced with permission from ref. 78. Copyright 2025, American Chemical Society.

presence of intramolecular charge transfer (ICT) in both probes and their products, while the energy gap (ΔE_{H-L}) analysis explained substituent-dependent spectral shifts (Fig. 19B). By providing a molecular-level rationale that aligns well with experimental observations, this work bridges theory and experiment, offering valuable design principles for developing next-generation ratiometric 1,8-naphthalimide probes with enhanced performance in H_2S sensing.

Very recently, Dvorak and co-workers investigated hydroxy-1,8-naphthalimide derivatives (**Nap-29** to **Nap-32**) as scaffolds for reaction-based fluorescent probes, leveraging their strong photo-acidity and excited-state proton transfer (ESPT) behaviour to achieve red-shifted emission (Fig. 20A).[78] These probes were carefully designed to assess the influence of hydroxyl positional isomerism and electrophilic recognition motifs on H_2S sensing. 2,4-Dinitrobenzenesulfonyl ester (DNBS) and 2,4-dinitrobenzene ether (DNBE) were employed as effective recognition motifs. **Nap-29** with a DNBS group displayed dual "turn-on" fluorescence bands at λ = 455 and 599 nm upon H_2S-triggered nucleophilic aromatic substitution reaction, with rapid response kinetics ($k \approx 8.2 \times 10^2$ M^{-1} s^{-1}) and a detection limit of 3.34 μM (Fig. 20B and C). Comparative studies showed that **Nap-31** exhibited higher sensitivity than **Nap-29**, owing to the greater stability of its 4-naphtholate intermediate, although it did not display dual ESPT emission. **Nap-30** served as a mechanistic control, confirming that nucleophilic substitution at the naphthalene ring requires unnaturally high H_2S concentrations, while **Nap-32** showed lower sensitivity but improved selectivity over biothiols such as cysteine and glutathione. Importantly, confocal imaging in MDA-MB-231 cells validated the cellular applicability of **Nap-29**, with significant fluorescence enhancement correlating to intracellular H_2S levels and minimal cytotoxicity (Fig. 20D). This systematic structure–function analysis demonstrates that hydroxyl positioning and recognition-group chemistry are key determinants of ESPT efficiency, fluorescence output, sensitivity, and selectivity, providing guiding principles for designing next-generation H_2S probes with optimized red-shifted emission, reactivity, and biological compatibility.

3. Conclusions and outlook

In this review, we have provided a comprehensive overview of recent progress in the design and development of reactivity-based 1,8-naphthalimide fluorescent probes for H_2S detection. These systems employ a variety of sensing strategies-including nitro/azide reduction, thiolysis-mediated deprotection, nucleophilic substitution, and excited-state proton transfer (ESPT), each offering distinct mechanistic advantages. Table 1 summarizes the key sensing properties of the reported 1,8-naphthalimide-based chemosensors. Throughout the review, we emphasized how specific structural modifications influence sensing pathways, selectivity, sensitivity, and functional performance in biological and environmental settings. Collectively, these insights underscore the versatility of the 1,8-naphthalimide scaffold as a robust platform for constructing high-performance H_2S probes. By consolidating current developments and highlighting structure–function relationships, this review aims to serve as a valuable resource for researchers in chemical sensing, bioimaging, and analytical chemistry.

Despite significant advances, several challenges remain before these probes can be fully translated into practical applications. Most reported systems rely on simple turn-on fluorescence, which, although sensitive, can suffer from background interference. Greater emphasis on ratiometric probe design, providing internal self-calibration, greatly enhances quantitative reliability. Furthermore, while ICT modulation dominates current strategies, expanding into dual-mode (electrochemical–optical) and ESPT- or FRET-based platforms could improve selectivity and performance

Table 1 Summary of sensing properties of the 1,8-naphthalimide-based H_2S chemosensors discussed in this article (NR = not reported)

Probe	Product	Medium	LoD	Reaction time	Ref.
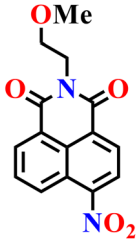 Nap-1	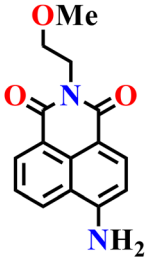	Aqueous buffer (50 mM PIPES, 100 mM KCl, pH 7.4)	5–10 μM	90 min	45
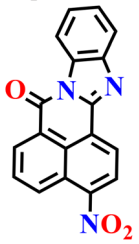 Nap-2		DMSO–H_2O (9 : 1) medium	μM	20 min	57
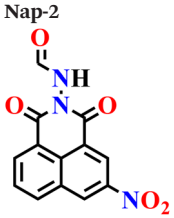 Nap-3	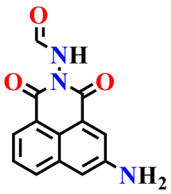	DMSO	8.1 μM	NR	58
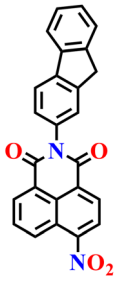 Nap-4	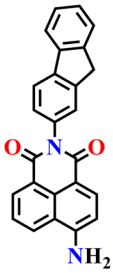	DMSO 0.5%; PBS 99.5%	14 mM	NR	59
 Nap-5	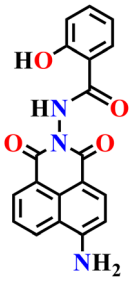	0.25% DMSO : 99.75% PBS	12.33 nM	20 h	60
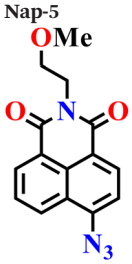 Nap-6	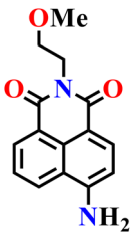	Aqueous buffer (50 mM PIPES, 100 mM KCl, pH 7.4)	1–5 μM	45 min	45

Table 1 *(continued)*

Probe	Product	Medium	LoD	Reaction time	Ref.
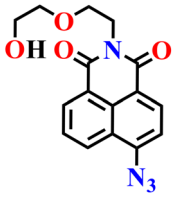 Nap-7		Aqueous DMSO solution (H_2O–DMSO, pH 7.4)	0.37 μM and 1.4 ppb in real samples	15 min	61
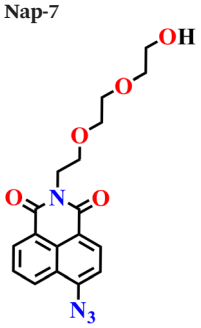 Nap-8	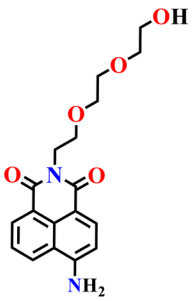	PBS buffer (10 μM, pH 7.4)	Less than 0.3 μM	30 min	62
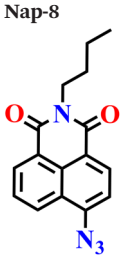 Nap-9	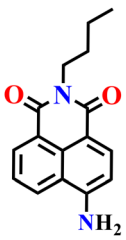	PBS buffer (10 μM, pH 7.4)	μM	30 min	62
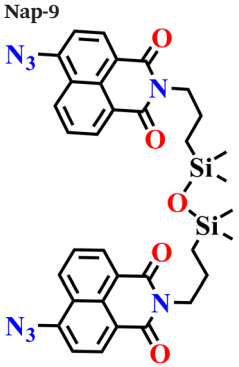 Nap-10	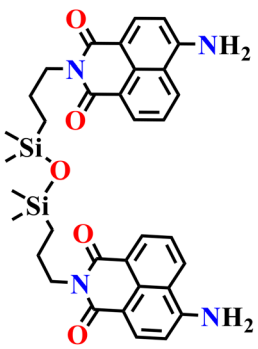	Aqueous solution (25 μM PBS buffer, pH = 7.4, containing 10% ethanol)	0.57 μM	12 min	63
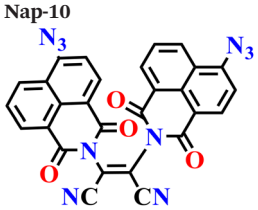 Nap-11	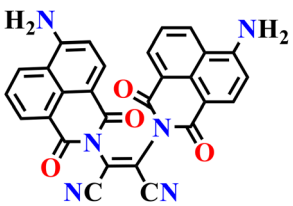	PBS : DMSO (1 : 1, v/v, pH 7.4)	1.5 μM	2 s	64
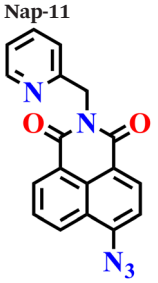 Nap-12		Acetonitrile/water (8 : 2 v/v)	1.2 μM.	~8–10 s	65

Table 1 *(continued)*

Probe	Product	Medium	LoD	Reaction time	Ref.
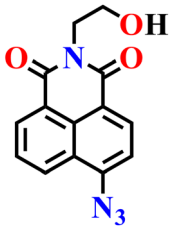 Nap-13		DMSO	1×10^{-7} M	10 s	66
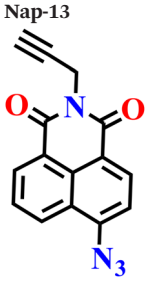 Nap-14		CH_3CN/PBS buffer (v : v = 1 : 1, 20 mmol L^{-1}, pH 7.4)	1.18 μM	3 min	67
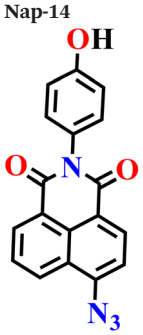 Nap-15	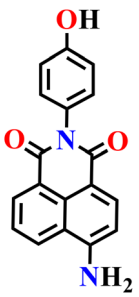	DMF/PBS solution (v/v, 7/3, pH 7.4, 20.0 mM)	0.085 μM	3 min	68
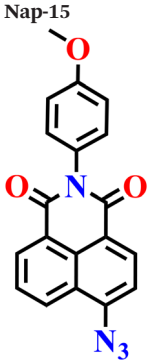 Nap-16	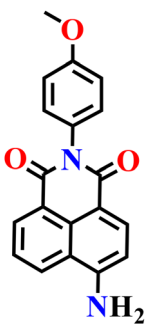	PBS buffer	17.4 nM	NR	69
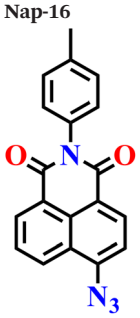 Nap-17	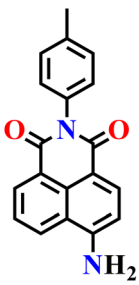	PBS buffer (pH 5.8–8.0)	0.085 μM	15 min	70

Table 1 *(continued)*

Probe	Product	Medium	LoD	Reaction time	Ref.
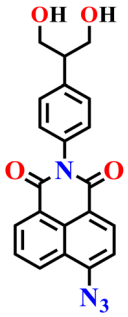 Nap-18	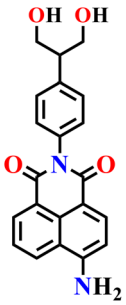	Ethanol/water	0.16 μmol L^{-1}	30 min	71
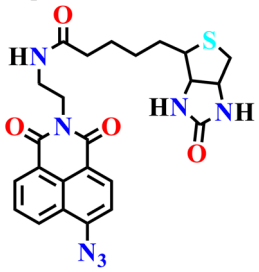 Nap-19	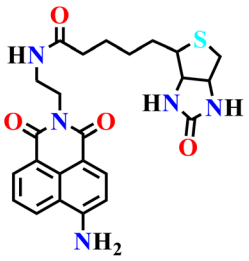	NR	NR	NR	72
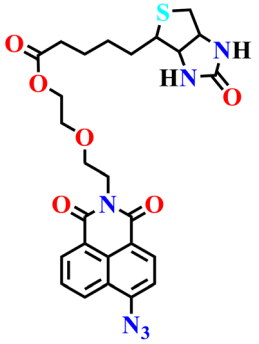 Nap-20	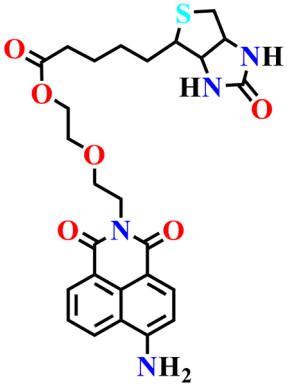	NR	NR	NR	72
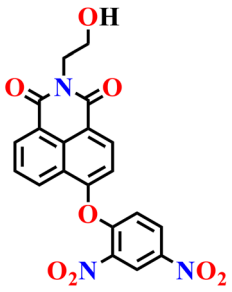 Nap-21	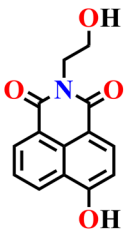	PBS/EtOH solution	1.54 μmol L^{-1}	120 min	73

Table 1 *(continued)*

Probe	Product	Medium	LoD	Reaction time	Ref.
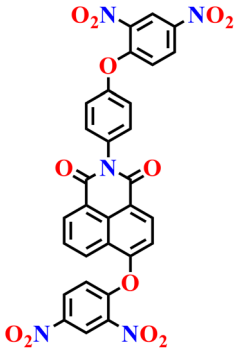 Nap-22	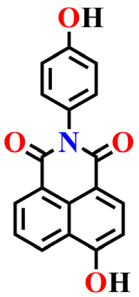	PBS/EtOH solution	1.40 μmol L^{-1}	120 min	73
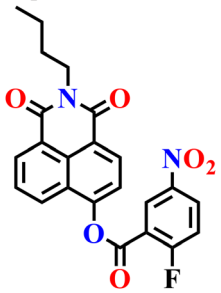 Nap-23	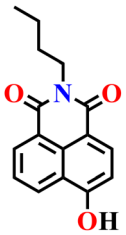	10 mM phosphate buffer solution (containing 1% DMSO as a co-solvent)	33 nM.	5 min	74
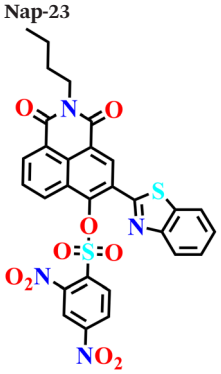 Nap-24	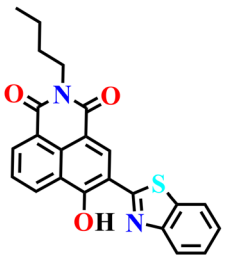	Aqueous solution (25 mM PBS, pH 7.4, mixed with 20% EtOH)	22.2 μM	2 min	75
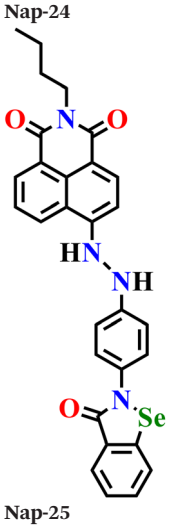 Nap-25	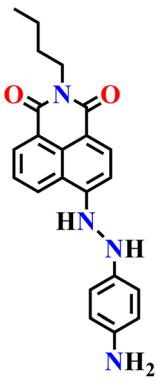	Mixture of PBS buffer (pH 7.4) and DMSO (10%)	0.129 μM	90 s	76

Table 1 *(continued)*

Probe	Product	Medium	LoD	Reaction time	Ref.
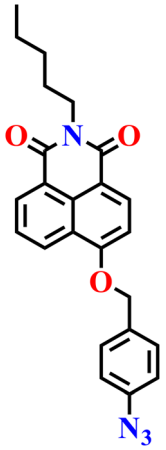 **Nap-26**	NR	NR	NR	NR	77
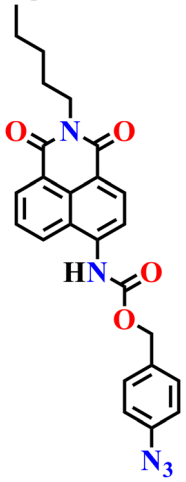 **Nap-27**	NR	NR	NR	NR	77
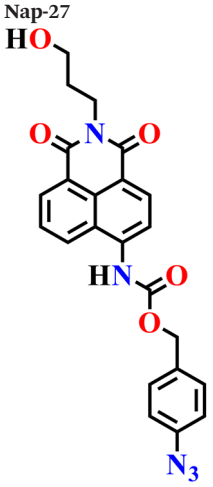 **Nap-28**	NR	NR	NR	NR	77

Table 1 *(continued)*

Probe	Product	Medium	LoD	Reaction time	Ref.
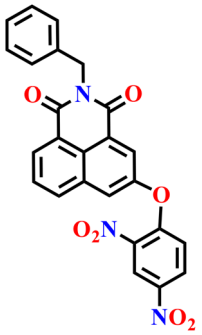 Nap-29	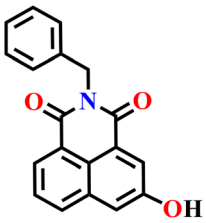	DMSO–phosphate buffer (0.01 M) at pH 7.4 (3 : 7, v/v)	3.34 μM	15 min	78
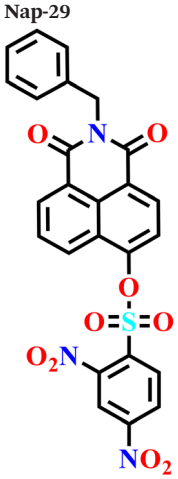 Nap-30	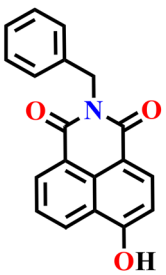	DMSO–phosphate buffer (0.01 M) at pH 7.4 (3 : 7, v/v)	μM	NR	78
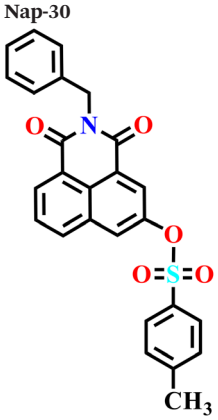 Nap-31	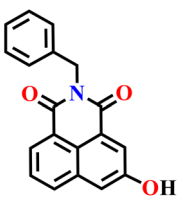	DMSO–phosphate buffer (0.01 M) at pH 7.4 (3 : 7, v/v)	μM	NR	78
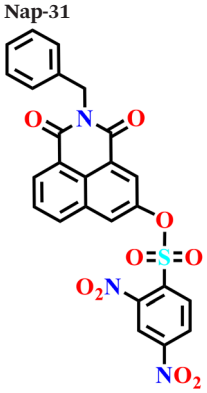 Nap-32	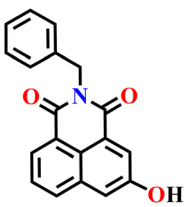	DMSO	μM	10 min	78

in complex media. Selectivity remains a persistent issue, especially in the presence of abundant endogenous biothiols like GSH and cysteine, which can compete with H_2S. Improved recognition motifs and strategic incorporation of electron-withdrawing groups may help minimize such cross-reactivity.

Reaction kinetics also warrant further optimization. Many existing probes respond slowly due to limited reactivity at aromatic trigger sites. Incorporating more reactive motifs—such as aliphatic amines, selenium-based groups, or strained electrophiles—could substantially accelerate response times. Although several probes now reach nanomolar detection limits, their stability and performance under physiologically relevant conditions must be strengthened for reliable *in vivo* imaging. Progressing from cell-level demonstrations to tissue and whole-animal imaging will require probes with enhanced aqueous solubility, high photostability, and compatibility with near-infrared or two-photon excitation for deeper tissue penetration and minimal autofluorescence.

Among the different probe types, thiolysis-based systems generally offer the fastest response but are more prone to interference from abundant biothiols, while reduction-based probes provide higher specificity toward H_2S but often respond more slowly. Nucleophilic substitution probes are synthetically simple yet more susceptible to false signals in thiol-rich environments. In contrast, ESPT- and FRET-based designs offer more stable or ratiometric outputs, making them better suited for accurate imaging in complex biological samples. Overall, each sensing strategy presents distinct strengths and limitations, underscoring the importance of selecting or designing probes based on the specific demands of the intended application.

In conclusion, 1,8-naphthalimide-based fluorescent probes represent a powerful and continually evolving platform for H_2S sensing. Continued innovation in probe design, targeting improved selectivity, faster kinetics, and advanced imaging capabilities, is expected to yield next-generation systems capable of real-time H_2S monitoring across diverse biological and environmental contexts. Looking forward, such probes hold significant promise for applications in disease diagnostics, redox biology, therapeutic monitoring, environmental pollutant analysis, and imaging-guided studies of sulfur-mediated signaling pathways. These opportunities highlight both the broad impact and the future potential of the developments summarized in this review.

Author contributions

M. K. Noushija: conceptualization, software, resources, visualization, funding acquisition, writing – original draft, A. V. Krishna: software, resources, visualization, writing – original draft. S. Shanmugaraju: conceptualization, software, resources, visualization, project administration, supervision, investigation, funding acquisition, writing – original draft, writing – review & editing.

Conflicts of interest

There are no conflicts to declare.

Data availability

No new data were generated or analysed as part of this review.

Acknowledgements

We gratefully acknowledge financial support from the Anusandhan National Research Foundation, India (EMEQ research grant EEQ/2023/000386 and CRG research grant CRG/2023/006085 awarded to SS), and from the Department of Science and Technology, Government of India (India-Japan Science and Technology Cooperation research grant DST/ICD/JSPS/2024/698 to SS).

Notes and references

1 R. Wang, *Trends Biochem. Sci.*, 2014, **39**, 227–232.
2 C. Mancuso, P. Navarra and P. Preziosi, *J. Neurochem.*, 2010, **113**, 563–575.
3 O. Kabil and R. Banerjee, *J. Biol. Chem.*, 2010, **285**, 21903–21907.
4 K. Qu, S. W. Lee, J. S. Bian, C.-M. Low and P.-H. Wong, *Neurochem. Int.*, 2008, **52**, 155–165.
5 C. Chen, H. Xin and Y. Zhu, *Acta Pharmacol. Sin.*, 2007, **28**, 1709–1716.
6 W. A. Pryor, *Am. J. Physiol.*, 2006, **291**, R491–R511.
7 D. R. Lide and H. P. R. Frederikse, *Handbook of Chemistry and Physics*, CRC Press, Boca Raton, FL, 76th edn, 1995.
8 G. Yang, L. Wu, B. Jiang, W. Yang, J. Qi, K. Cao, Q. Meng, A. K. Mustafa, W. Mu and S. Zhang, *Science*, 2008, **322**, 587–590.
9 N. Shibuya, M. Tanaka, M. Yoshida, Y. Ogasawara, T. Togawa, K. Ishii and H. Kimura, *Antioxid. Redox Signaling*, 2009, **11**, 703–714.
10 R. Hosoki, N. Matsuki and H. Kimura, *Biochem. Biophys. Res. Commun.*, 1997, **237**, 527–531.
11 K. Abe and H. Kimura, *J. Neurosci.*, 1996, **16**, 1066–1071.
12 L.-F. Hu, M. Lu, P. T. Hon Wong and J.-S. Bian, *Antioxid. Redox Signaling*, 2011, **15**, 405–419.
13 N. S. Lawrence, J. Davis and R. G. Compton, *Talanta*, 2000, **52**, 771–784.
14 M. M. Gadalla and S. H. Snyder, *J. Neurochem.*, 2010, **113**, 14–26.
15 M. Lee, C. Schwab, S. Yu, E. McGeer and P. L. McGeer, *Neurobiol. Aging*, 2009, **30**, 1523–1534.
16 E. Jw, *Proc. Natl. Acad. Sci. U. S. A.*, 2007, **104**, 15560–15565.
17 K. Qu, C. P. L. H. Chen, B. Halliwell, P. K. Moore and P. T.-H. Wong, *Stroke*, 2006, **37**, 889–893.
18 A. Sivarajah, M. C. McDonald and C. Thiemermann, *Shock*, 2006, **26**, 154–161.
19 A. Ichinohe, T. Kanaumi, S. Takashima, Y. Enokido, Y. Nagai and H. Kimura, *Biochem. Biophys. Res. Commun.*, 2005, **338**, 1547–1550.

20 H. Yan, J. Du and C. Tang, *Biochem. Biophys. Res. Commun.*, 2004, **313**, 22–27.
21 P. Kamoun, M. Belardinelli, A. Chabli, K. Lallouchi and B. Chadefaux-Vekemans, *Am. J. Med. Genet., Part A*, 2003, **116**, 310–311.
22 K. Eto, T. Asada, K. Arima, T. Makifuchi and H. Kimura, *Biochem. Biophys. Res. Commun.*, 2002, **293**, 1485–1488.
23 J. E. Doeller, T. S. Isbell, G. Benavides, J. Koenitzer, H. Patel, R. P. Patel, J. R. Lancaster Jr, V. M. Darley-Usmar and D. W. Kraus, *Anal. Biochem.*, 2005, **341**, 40–51.
24 T. Ubuka, *J. Chromatogr., B*, 2002, **781**, 227–249.
25 N. S. Lawrence, J. Davis, L. Jiang, T. G. J. Jones, S. N. Davies and R. G. Compton, *Electroanalysis*, 2000, **12**, 1453–1460.
26 J. Radford-Knoery and G. A. Cutter, *Anal. Chem.*, 1993, **65**, 976–982.
27 J. C. Savage and D. H. Gould, *J. Chromatogr. B: Biomed. Sci. Appl.*, 1990, **526**, 540–545.
28 G. K. Kolluru, X. Shen, S. C. Bir and C. G. Kevil, *Nitric Oxide*, 2013, **35**, 5–20.
29 L. D. Lavis and R. T. Raines, *ACS Chem. Biol.*, 2008, **3**, 142–155.
30 E. L. Que, D. W. Domaille and C. J. Chang, *Chem. Rev.*, 2008, **108**, 1517–1549.
31 P. Wardman, *Free Radical Biol. Med.*, 2007, **43**, 995–1022.
32 J. Pan, J. Xu, Y. Zhang, L. Wang, C. Qin, L. Zeng and Y. Zhang, *Spectrochim. Acta, Part A*, 2016, **168**, 132–138.
33 J. Hong, W. Feng and G. Feng, *Sens. Actuators, B*, 2018, **262**, 837–844.
34 W. Luo, H. Xue, J. Ma, L. Wang and W. Liu, *Anal. Chim. Acta*, 2019, **1077**, 273–280.
35 K. Zhong, L. Chen, X. Yan, Y. Tang, S. Hou, X. Li and L. Tang, *Dyes Pigm.*, 2020, **182**, 108656.
36 H. Zhang, X. Yue, W. Li, W. Chen, Y. Wang, X. Li, Y. Ye and X. Song, *Sens. Actuators, B*, 2021, **331**, 129394.
37 K. Liu, C. Liu, H. Shang, M. Ren and W. Lin, *Sens. Actuators, B*, 2018, **256**, 342–350.
38 W. Chen, S. Chen, B. Zhou, H. Wang, X. Song and H. Zhang, *Dyes Pigm.*, 2015, **113**, 596–601.
39 W. Xuan, C. Sheng, Y. Cao, W. He and W. Wang, *Angew. Chem., Int. Ed.*, 2012, **51**, 2282–2284.
40 W.-X. Wang, Z.-Q. Wang, Z.-K. Tan, G.-J. Mao, D.-H. Chen and C.-Y. Li, *Analyst*, 2022, **147**, 2712–2717.
41 X.-G. Chen, Y. Mei, H. Li and Q.-H. Song, *Sens. Actuators, B*, 2022, **354**, 131202.
42 S.-J. Li, Y.-F. Li, H.-W. Liu, D.-Y. Zhou, W.-L. Jiang, J. Ou-Yang and C.-Y. Li, *Anal. Chem.*, 2018, **90**, 9418–9425.
43 R. M. Duke, E. B. Veale, F. M. Pfeffer, P. E. Kruger and T. Gunnlaugsson, *Chem. Soc. Rev.*, 2010, **39**, 3936–3953.
44 W. W. Stewart, *Nature*, 1981, **292**, 17–21.
45 L. A. Montoya and M. D. Pluth, *Chem. Commun.*, 2012, **48**, 4767–4769.
46 Z. Xu, L. Xu, J. Zhou, Y. Xu, W. Zhu and X. Qian, *Chem. Commun.*, 2012, **48**, 10871–10873.
47 X. Cao, W. Lin, K. Zheng and L. He, *Chem. Commun.*, 2012, **48**, 10529–10531.
48 C. Liu, J. Pan, S. Li, Y. Zhao, L. Y. Wu, C. E. Berkman, A. R. Whorton and M. Xian, *Angew. Chem., Int. Ed.*, 2011, **50**, 10327.
49 X. Wu, H. Li, Y. Kan and B. Yin, *Dalton Trans.*, 2013, **42**, 16302–16310.
50 C. Kar and G. Das, *J. Photochem. Photobiol., A*, 2013, **251**, 128–133.
51 X.-F. Yang, L. Wang, H. Xu and M. Zhao, *Anal. Chim. Acta*, 2009, **631**, 91–95.
52 M. G. Choi, S. Cha, H. Lee, H. L. Jeon and S.-K. Chang, *Chem. Commun.*, 2009, 7390–7392.
53 G. Kim, E. Jang, A. M. Page, T. Ding, K. A. Carlson and H. Cao, *RSC Adv.*, 2016, **6**, 95920–95924.
54 T. Annaka, N. Nakata and A. Ishii, *New J. Chem.*, 2019, **43**, 11643–11652.
55 Q. Wu, F. Huo, J. Wang and C. Yin, *Spectrochim. Acta, Part A*, 2020, **238**, 118437.
56 X. Shen, C. B. Pattillo, S. Pardue, S. C. Bir, R. Wang and C. G. Kevil, *Free Radical Biol. Med.*, 2011, **50**, 1021–1031.
57 A. Bamesberger, G. Kim, J. Woo and H. Cao, *J. Fluoresc.*, 2015, **25**, 25–29.
58 S. Naha, S. P. Wu and S. Velmathi, *RSC Adv.*, 2020, **10**, 8751–8759.
59 M. Ranjana, M. S. Shrilaxmi, A. Bera, D. Sunil, Y. N. Sudhakar, D. Upadhya, S. G. Dastidar, S. R. Vennapusa and S. D. Kulkarni, *Microchem. J.*, 2025, **215**, 114060.
60 M. Ranjana, N. N. Kashyap, D. Sunil, A. Bera, P. K. Mitra, P. P. Yegneswaran, Y. N. Sudhakar, D. Upadhya, S. D. Kulkarni and S. R. Vennapusa, *Analyst*, 2025, **150**, 5245.
61 Y. Guo, T. Zeng, G. Shi, Y. Cai and R. Xie, *RSC Adv.*, 2014, **4**, 33626–33628.
62 S. A. Choi, C. S. Park, O. S. Kwon, H. K. Giong, J. S. Lee, T. H. Ha and C. S. Lee, *Sci. Rep.*, 2016, **6**, 1–10.
63 X. Wang, Y. Zuo, Y. Zhang, T. Yanga and W. Lin, *Anal. Methods*, 2020, **12**, 1064–1069.
64 D. Jothi, S. Munusamy and S. K. Iyer, *J. Photochem. Photobiol., A*, 2021, **420**, 2–9.
65 D. Jothi and S. K. Iyer, *J. Photochem. Photobiol., A*, 2022, **427**, 113802.
66 Y. Yan, S. Zhu, Z. Chen and Y. Ji, *J. Appl. Spectrosc.*, 2022, **89**, 191–200.
67 Z. Jihua, Z. Hao, L. Min, L. Jingjiang, L. Yuan, Q. Zhengjun and W. Xicun, *Chin. J. Org. Chem.*, 2020, **40**, 1043–1049.
68 J. Zhu, C. Miao and X. Wang, *J. Photochem. Photobiol., A*, 2023, **440**, 114659.
69 Y. Zhang and L. Zhang, *Microchem. J.*, 2020, **159**, 105394.
70 A. Dandić, M. Samardžić, M. Budetić, I. D. Panić, I. Drenjančević, N. Kolobarić, G. Mikle, B. Kovács and A. Széchenyi, *J. Fluoresc.*, 2024, **35**, 1–9.
71 A. Széchenyi, M. Budetić, M. Samardžić, M. Stanković, I. Drenjančević, N. Kolobarić, B. Kovács, B. Lemli, G. Mikle and A. Dandić, *J. Fluoresc.*, 2025, DOI: 10.1007/s10895-025-04582-7.
72 A. Huang, D. Wu, W. Hao and H. He, *Spectrochim. Acta, Part A*, 2025, **338**, 126202.

73 Y. Ma, J. Zhang and H. Qu, *Chem. Res. Chin. Univ.*, 2019, **35**, 5–11.
74 L. Zhou, G. Yuan and S. Hu, *J. Appl. Spectrosc.*, 2020, **86**, 1071–1076.
75 K. Xu, L. He, Y. Yanga and W. Lin, *New J. Chem.*, 2019, **43**, 2865–2869.
76 C. Zhang, L. Zhang, Y. Li, Z. Ren, L. Li, Y. Zhang, Y. Li and C. Liu, *J. Mol. Struct.*, 2021, **1250**, 131777.
77 A. Huang, Y. Zhou, Y. Liang, Q. Liu, W. Hao, Z. Xia, D. Wu and H. He, *J. Fluoresc.*, 2024, **35**, 1–8.
78 T. Dvorak, S. Cheku, L. Borer, H. Hernandez-Sandoval, K. A. Carlson and H. Cao, *ACS Omega*, 2025, **10**, 31138–31146.